

Hamiltonian Simulation Algorithms for Near-Term Quantum Hardware

Laura Clinton^{*1,2}, Johannes Bausch^{†1,3}, and Toby Cubitt^{‡1}

¹PhaseCraft Ltd.

²Department of Computer Science, University College London

³Department of Applied Mathematics and Theoretical Physics,
University of Cambridge

March 2020

The quantum circuit model is the de-facto way of designing quantum algorithms. Yet any level of abstraction away from the underlying hardware incurs overhead. In the era of near-term, noisy, intermediate-scale quantum (NISQ) hardware with severely restricted resources, this overhead may be unjustifiable. In this work, we develop quantum algorithms for Hamiltonian simulation “one level below” the circuit model, exploiting the underlying control over qubit interactions available in principle in most quantum hardware implementations. This sub-circuit model approach significantly reduces both the run-time of the algorithm, and the propagation of errors during the algorithm – particularly important when resources are too limited to perform active error correction.

To quantify the benefits of this approach, we apply it to a canonical example: time-dynamics simulation of the 2D spin Fermi-Hubbard model. We derive analytic circuit identities for efficiently synthesising multi-qubit evolutions from two-qubit interactions. Combined with new error bounds for Trotter product formulas tailored to the non-asymptotic regime, a novel low-weight fermion encoding, and a careful analysis of error propagation in the sub-circuit model algorithm, we improve upon the previous best methods for Hamiltonian simulation by multiple orders of magnitude. For example, for a 5×5 Fermi-Hubbard lattice – already challenging on classical supercomputers – we reduce the circuit-depth-equivalent from 800,160 to 2960. This brings Hamiltonian simulation, previously beyond reach of current hardware for non-trivial examples, significantly closer to being feasible in the NISQ era.

^{*}laura@phasecraft.io

[†]johannes@phasecraft.io

[‡]toby@phasecraft.io

Contents

1	Extended Overview	3
1.1	Introduction	3
1.2	Encoding the Fermi-Hubbard Hamiltonian	6
1.3	Tighter Error Bounds for Trotter Product Formulas	9
1.4	Sub-Circuit-Model Synthesis of Trotter Layers	12
1.5	Benchmarking the Sub-Circuit-Model	13
1.6	Sub-Circuit Algorithms on Noisy Hardware	15
1.7	Conclusions	18
2	Sub-Circuit-Model and Cost Model	19
3	Decomposing Local Trotter Steps	20
3.1	Analytic Pulse Sequence Identities	20
3.2	Pulse-Time Bounds on Analytic Decompositions	22
3.3	Optimality	24
4	Suzuki-Trotter Formulae Error Bounds	27
4.1	Existing Trotter Bounds	27
4.2	Hamiltonian Simulation by Trotterisation	27
4.3	Error Analysis of Higher-Order Formulae	28
4.4	Explicit Summation of Trotter Stage Coefficients	33
4.5	Commutator Bounds	34
4.6	A Taylor Bound on the Taylor Bound	38
5	Spectral Norm of Fermionic Hopping Terms	40
6	Simulating Fermi-Hubbard via Sub-Circuit Algorithms	42
6.1	Overview and Benchmarking of Analysis	42
6.2	The Fermi-Hubbard Hamiltonian and Fermionic Encodings	43
6.3	Choice of Trotter Layers	44
6.4	Analytic Run-Time Bounds for Simulating Fermi Hubbard	47
6.5	Trivial Stochastic Error Bound	50
6.6	Error Mapping under Fermionic Encodings	51
6.7	Numeric Results	52
7	Simulating Fermi-Hubbard with Three Trotter Layers	55
7.1	Further Circuit Decompositions	55
7.2	Regrouping Interaction Terms	56

1 Extended Overview

1.1 Introduction

Quantum computing is on the cusp of entering the era in which quantum hardware can no longer be simulated effectively classically, even on the world’s biggest supercomputers [Vil+20; BJS11; AA10; BMS17; HM17]. Google recently achieved the first so-called “quantum supremacy” milestone demonstrating this [Goo+19a]. Whilst reaching this milestone is an impressive experimental physics achievement, the very definition of this goal allows it to be a demonstration that has no useful practical applications [Pre12]. The recent Google results are of exactly this nature. By far the most important question for quantum computing now is to determine whether there are useful applications of this class of noisy, intermediate-scale quantum (NISQ) hardware [Pre18].

However, current quantum hardware is still extremely limited, with ≈ 50 qubits capable of implementing quantum circuits up to a gate depth of ≈ 20 [Goo+19a]. This is far too limited to run useful instances of even the simplest textbook quantum algorithms, let alone implement the error correction and fault-tolerance required for large-scale quantum computations. Estimates of the number of qubits and gates required to run Shor’s algorithm on integers that cannot readily be factored on classical computers place it – and related number-theoretic algorithms – well into the regime of requiring a fully scalable, fault-tolerant quantum computer [HRS16; Roe+17]. Studies of practically relevant combinatorial problems tell a similar story for capitalising on the quadratic speedup of Grover’s algorithm [Mon15]. Quantum computers are naturally well-suited for simulation of quantum many-body systems [Fey82; Llo96] – a task that is notoriously difficult on classical computers. Quantum simulation is likely to be one of the first practical applications of quantum computing. But, whilst the number of qubits required to run interesting quantum simulations may be lower than for other applications, careful studies of the gate counts required for a quantum chemistry simulation of molecules that are not easily tractable classically [Goo+19a], or for simple condensed matter models [Kiv+19], remain far beyond current hardware.

Sub-circuit-model algorithms. With such severely resource-constrained hardware, squeezing every ounce of performance out of it is crucial. The quantum circuit model is the standard way to design quantum algorithms, and quantum gates and circuits provide a highly convenient abstraction of quantum hardware. Circuits sit at a significantly lower level of abstraction than even assembly code in classical computing. But any layer of abstraction sacrifices some overhead for the sake of convenience. The quantum circuit model is no exception.

In the underlying hardware, quantum gates are typically implemented by controlling interactions between qubits. E.g. by changing voltages to bring superconducting qubits in and out of resonance; or by laser pulses to manipulate the internal states of trapped ions. By restricting to a fixed set of standard gates, the circuit model abstracts away the full capabilities of the underlying hardware. In

the NISQ era, it is not clear this sacrifice is justified. The Solovay-Kitaev theorem tells us that the overhead of any particular choice of universal gate set is at most poly-logarithmic [Kit97; DN05]. But when the available circuit depth is limited to ≈ 20 , even a constant factor improvement could make the difference between being able to run an algorithm on current hardware, and being beyond the reach of foreseeable hardware.

The advantages of designing quantum algorithms “one level below” the circuit model are particularly acute in the case of Hamiltonian time-dynamics simulation. To simulate evolution under a many-body Hamiltonian $H = \sum_{\langle i,j \rangle} h_{ij}$, the basic Trotterization algorithm [Llo96; NC10] repeatedly time-evolves the system under each individual interaction h_{ij} for a small time-step δ ,

$$e^{-iHT} \simeq \prod_{n=0}^{T/\delta} \left(\prod_{\langle i,j \rangle} e^{-ih_{ij}\delta} \right). \quad (1)$$

To achieve good precision, δ must be small. (See Section 4 for a mathematically precise treatment.) In the circuit model, each $e^{-ih_{ij}\delta}$ Trotter step necessarily requires at least one quantum gate to implement. Thus the required circuit depth – and hence the total run-time – is at least T/δ . Contrast this with the run-time if we were able to implement $e^{-ih_{ij}\delta}$ directly in time δ . The total run-time would then be T , which improves on the circuit model algorithm by a factor of $1/\delta$. This is “only” a constant factor improvement, in line with the Solovay-Kitaev theorem. But this “constant” can be very large; indeed, it diverges to ∞ as the precision of the algorithm increases.

It is unrealistic to assume the hardware can implement $e^{-ih_{ij}\delta}$ for any desired interaction h_{ij} and any time δ . The available interactions are typically limited to at most a handful of specific types, determined by the underlying physics of the device’s qubit and quantum gate implementations. And these interactions cannot be switched on and off arbitrarily fast, placing a limit on the smallest achievable value of δ . But the above simplistic analysis already indicates there may be large gains from designing algorithms to exploit the full hardware capabilities, rather than restricting to standard gates and circuits.

In this work, we develop more sophisticated techniques for synthesising many-body interactions out of the underlying one- and two-qubit interactions available in the quantum hardware (see Sections 1.4 and 3), and show that the type of gains discussed here can be achieved, even when we restrict to a conservative model of the underlying hardware capabilities (see Section 2).

Mitigating errors and noise. A major criticism of analogue computation (classical and quantum) is that it cannot cope with errors and noise. The ‘N’ in NISQ stands for “noisy”. Near-term hardware has few resources to spare even on basic error correction, let alone fault-tolerance. Indeed, near-term hardware may not even have the necessary capabilities. E.g. the intermediate measurements required for active error-correction are not possible in some of the current superconducting circuit hardware [Goo+19b, Sec. II]. Algorithms that cope well with errors and noise, and still give reasonable results without error correction or fault-tolerance, are thus critical for NISQ applications.

As well as potential gains in efficiency, designing algorithms “one level below” the circuit model can also in some cases reduce the impact of errors and noise during the algorithm. Again, this benefit is particularly acute in Hamiltonian simulation algorithms. If an error occurs on a qubit in a quantum circuit, a two-qubit gate acting on the faulty qubit can spread the error to a second qubit. In the absence of any error-correction or fault-tolerance, errors can spread to an additional qubit with each two-qubit gate applied, so that after circuit depth n the error can spread to all n qubits.

In the circuit model, each $e^{-ih_{ij}\delta}$ Trotter step requires at least one two-qubit gate. So a single error can be spread throughout the quantum computer after simulating time-evolution for time as short as δn . However, if a two-qubit interaction $e^{-ih_{ij}\delta}$ is implemented directly, one would intuitively expect it to only “spread the error” by a small amount δ for each such time-step. Thus we might expect it to take time $O(n)$ before the error can propagate to all n qubits – a factor of $1/\delta$ improvement.¹ This intuition can be made mathematically rigorous (see Sections 1.6 and 4).

Hamiltonian simulation. The Fermi-Hubbard model is believed to capture, in a simplified toy model, key aspects of high-temperature superconductors, which are still less well understood theoretically than their low-temperature brethren. Its Hamiltonian is given by a combination of on-site and hopping terms:

$$H_{\text{FH}} := \sum_{i=1}^N h_{\text{on-site}}^{(i)} + \sum_{i < j, \sigma} h_{\text{hopping}}^{(i,j,\sigma)} := u \sum_{i=1}^N a_{i\uparrow}^\dagger a_{i\uparrow} a_{i\downarrow}^\dagger a_{i\downarrow} + v \sum_{i < j, \sigma} \left(a_{i\sigma}^\dagger a_{j\sigma} + a_{j\sigma}^\dagger a_{i\sigma} \right). \quad (2)$$

describing electrons with spin $\sigma = \uparrow$ or \downarrow hopping between neighbouring sites on a lattice, with an on-site interaction between opposite-spin electrons at the same site. The Fermi-Hubbard model serves as a particularly good test-bed for NISQ Hamiltonian simulation algorithms for a number of reasons [Bau+20a, Sec. IV], beyond the fact that it is a scientifically interesting model in its own right:

1. The Fermi-Hubbard model was a famous, well-studied condensed matter model long before quantum computing was proposed. It is therefore less open to the criticism of being an artificial problem tailored to fit the algorithm.
2. It is a fermionic model, which poses particular challenges for simulation on (qubit-based) quantum computers. Most of the proposed practical applications of quantum simulation involve fermionic systems, either in quantum chemistry or materials science. So achieving quantum simulation of fermionic models is an important step on the path to practical quantum computing applications.

¹Another way of viewing this is that, in the circuit model, the Lieb-Robinson velocity [LR72] at which effects propagate in the system is always $O(1)$, regardless of what unitary dynamics is being implemented by the overall circuit. In contrast, the Trotterized Hamiltonian evolution has the same Lieb-Robinson velocity as the dynamics being simulated: $O(1/\delta)$ in the same units.

3. There have been over three decades of research developing ever-more-sophisticated classical simulations of Fermi-Hubbard-model physics [LeB+15]. This gives clear benchmarks against which to compare quantum algorithms. And it reduces the likelihood of there being efficient classical algorithms, which haven't been discovered because little interest or effort has been devoted to the model.

The state-of-the-art quantum circuit-model algorithm for simulating the time dynamics of the 2D Fermi-Hubbard model on an 8×8 lattice requires $\approx 10^7$ Toffoli gates [Kiv+19, Sec. C: Tb. 2]. This includes the overhead for fault-tolerance, which is necessary for the algorithm to achieve reasonable precision with the gate fidelities available in current and near-term hardware. But it additionally incorporates performing phase estimation, which is a significant additional contribution to the gate count. Thus, although this result is indicative of the scale required for standard circuit-model Hamiltonian simulation, a direct comparison of this result with time-dynamics simulation would be unfair. Using readily applicable Trotter error bounds from the literature [Chi+17], with the best choice of fermion encoding in the preexisting literature [VC05], we calculate that one can achieve a Fermi-Hubbard time-dynamics simulation on a 5×5 square lattice, up to time $T = 7$ and to within 10% accuracy, using 50 qubits and a circuit depth of 800,000 two-qubit gates. This estimate assumes the effects of decoherence and errors in the circuit can be neglected, which is certainly over-optimistic.

By designing a quantum algorithm “one level below” the circuit model (Section 1.4), exploiting a new fermion encoding specifically designed for this type of algorithm (Section 1.2 and [DK20]), deriving new tighter error bounds on the higher-order Trotter expansions that account for all constant factors (Section 1.3), and by analysing the impact and rate of spread of decoherence-induced errors in the resulting algorithm (Section 1.6 and [Bau+20b]), we improve on this by multiple orders of magnitude even in the presence of decoherence. Specifically, we show that a 5×5 Fermi-Hubbard time-dynamics simulation up to time $T = 7$ can be performed to 10% accuracy with ≈ 50 qubits and the equivalent of circuit depth 3,000. This brings it significantly closer to being within reach of near-term NISQ hardware. Table 1 compares these results, showing how the combination of sub-circuit-model algorithms, better fermion encoding, and tighter Trotter bounds successively reduce the time cost of the simulation algorithm.

1.2 Encoding the Fermi-Hubbard Hamiltonian

To simulate fermionic systems on a quantum computer, one must encode the fermionic Fock space into qubits. There are many encodings in the literature [JW28] but we confine our analysis to two: the Verstraete-Cirac (VC) encoding [VC05], and the low-weight (LW) encoding recently introduced in [DK20]. We have selected these two encodings as they minimise the maximum Pauli weight of the encoded interactions, which is a key factor in the efficiency of our sub-circuit-model algorithms: weight-4 (VC) and weight-3 (LW), respectively. By comparison, the classic Jordan-Wigner transformation [JW28] results in a maximum Pauli weight that scales as

Gate Decomposition	Trotter Error Bounds	Encoding	$\mathcal{T}_{\text{cost}}(\mathcal{P}_p(\delta_0)^{T/\delta_0})$
Standard Sequence	Childs et al. [Chi+17, Prop. F.4.]	VC	800 160
	this paper	VC	80 810
		LW	65 418
Sub-circuit Sequence	this paper	VC	12 582
		LW	2 960

Table 1: A comparison of the best achievable $\mathcal{T}_{\text{cost}}(\mathcal{P}_p(\delta_0)^{T/\delta_0})$ for lattice size $L \times L$ with $L = 5$, overall simulation time $T = 7$ and target Trotter error $\epsilon_{\text{target}} = 0.1$, with $\Lambda = 5$ fermions and coupling strengths $|u|, |v| \leq r = 1$. Obtained by minimising over product formulas up to 4th order. In either gate decomposition case—sub-circuit sequences *and* conjugation—we count single-qubit rotations as a free resource; they do not contribute to $\mathcal{T}_{\text{cost}}$. Two-qubit unitaries are counted by their respective pulse lengths.

$O(L)$ with the lattice size L ; the Bravyi-Kitaev encoding [BK02] has interaction terms of weight $O(\log L)$; and the Bravyi-Kitaev superfast encoding [BK02] results in weight-8 interactions. (See Section 6 for more details).

Under the LW encoding, the fermionic operators in Eq. (2) are mapped to operators on qubits arranged on two stacked square grids of qubits (one corresponding to the spin up, and one to the spin down sector, as shown in Fig. 1d), augmented by a face-centered ancilla in a checkerboard pattern, with an enumeration explained in Fig. 1a.

The on-site, horizontal and vertical local terms in the Fermi-Hubbard Hamiltonian Eq. (2) are mapped under this encoding to qubit operators as follows:

$$\begin{aligned}
h_{\text{on-site}}^{(i)} &\rightarrow \frac{u}{4} (\mathbb{1} - Z_{i\uparrow}) (\mathbb{1} - Z_{i\downarrow}) \\
h_{\text{hopping,hor}}^{(i,j,\sigma)} &\rightarrow \frac{v}{2} \left(X_{i,\sigma} X_{j,\sigma} Y_{f_{ij},\sigma} + Y_{i,\sigma} Y_{j,\sigma} Y_{f_{ij},\sigma} \right) \\
h_{\text{hopping,vert}}^{(i,j,\sigma)} &\rightarrow \frac{v}{2} (-1)^{g(i,j)} \left(X_{i,\sigma} X_{j,\sigma} X_{f_{ij},\sigma} + Y_{i,\sigma} Y_{j,\sigma} X_{f_{ij},\sigma} \right),
\end{aligned}$$

where qubit f_{ij}' is the face-centered ancilla closest to vertex (i, j) , and $g(i, j)$ indicates an associated sign choice in the encoding, as explained in [DK20].

If the VC encoding is used, the fermionic operators in Eq. (2) are mapped to qubits arranged on two stacked square grids of qubits (again with one corresponding to spin up, the other to spin down, as shown in Fig. 2), augmented by an ancilla qubit for each data qubit and with an

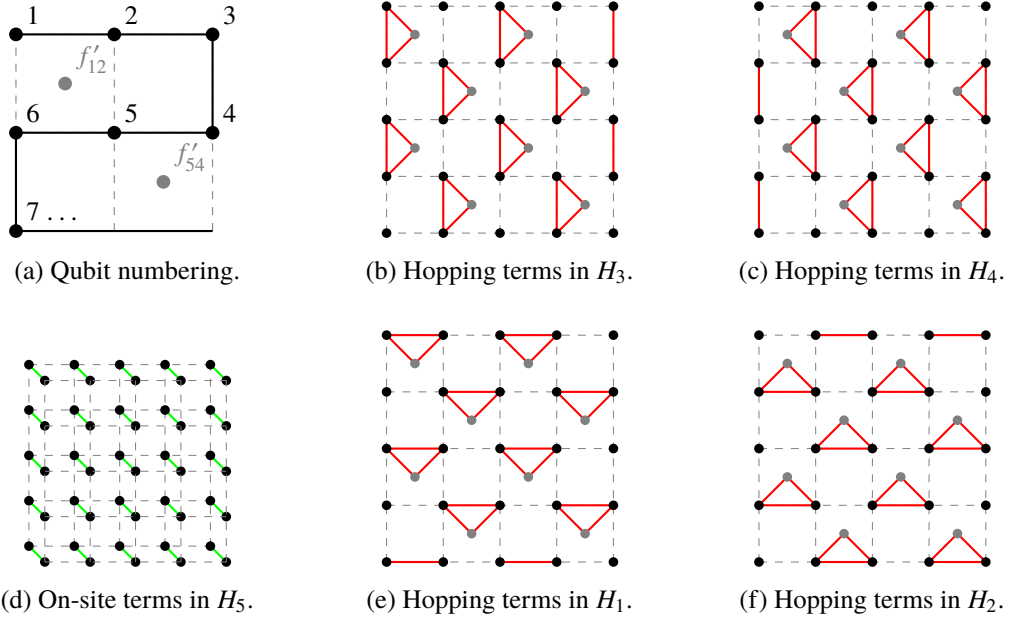


Figure 1: LW encoding: qubit enumeration, and five mutually non-commuting interaction layers.

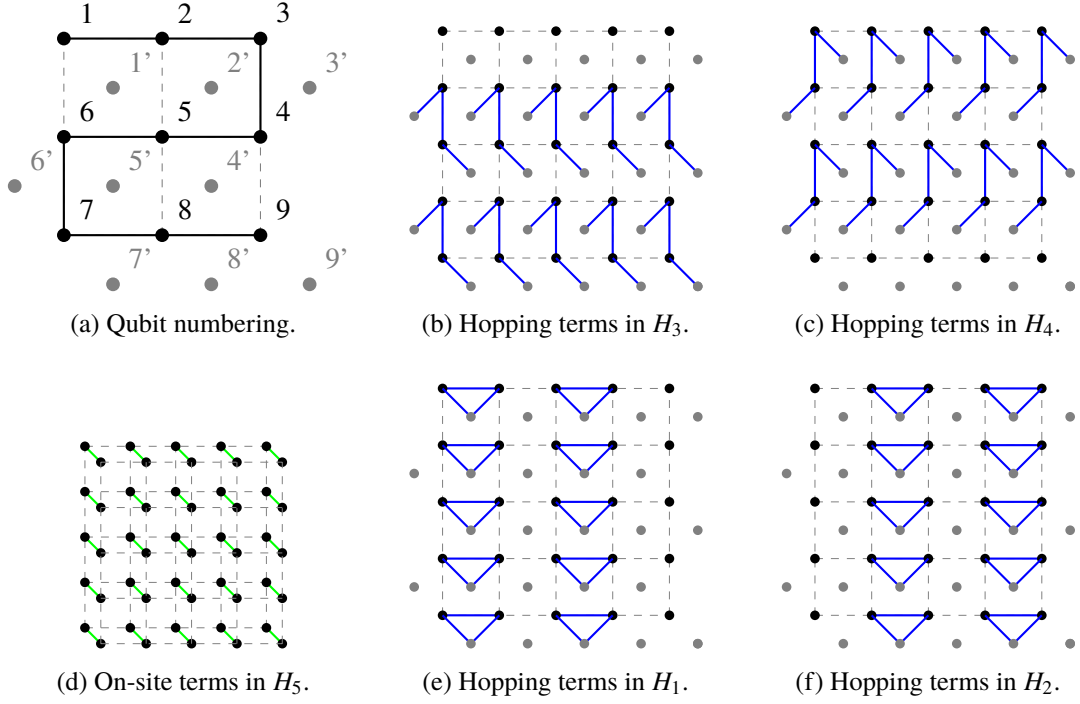


Figure 2: VC encoding: qubit enumeration, and five mutually non-commuting interaction layers.

enumeration explained in Fig. 2a. In this case the on-site, horizontal and vertical local terms are mapped to

$$\begin{aligned} h_{\text{on-site}}^{(i)} &\rightarrow \frac{u}{4} (\mathbb{1} - Z_{i\uparrow}) (\mathbb{1} - Z_{i\downarrow}) \\ h_{\text{hopping,hor}}^{(i,j,\sigma)} &\rightarrow \frac{v}{2} (X_{i,\sigma} Z_{i',\sigma} X_{j,\sigma} + Y_{i,\sigma} Z_{i',\sigma} Y_{j,\sigma}) \\ h_{\text{hopping,vert}}^{(i,j,\sigma)} &\rightarrow \frac{v}{2} (X_{i,\sigma} Y_{i',\sigma} Y_{j,\sigma} X_{j',\sigma} - Y_{i,\sigma} Y_{i',\sigma} X_{j,\sigma} X_{j',\sigma}), \end{aligned}$$

where i' indicates the ancilla qubit associated with qubit i .

In both encodings, we partition the resulting Hamiltonian H – a sum of on-site, horizontal and vertical qubit interaction terms on the augmented square lattice – into $M = 5$ layers $H = H_1 + H_2 + H_3 + H_4 + H_5$, as shown in Figs. 1 and 2. The Hamiltonians for each layer do not commute with one another. Each layer is a sum of mutually-commuting local terms acting on disjoint subsets of the qubits. For instance, $H_5 = \sum_i h_{\text{on-site}}^{(i)}$ is a sum of all the two-local, non-overlapping, on-site terms.

1.3 Tighter Error Bounds for Trotter Product Formulas

There are by now a number of sophisticated quantum algorithms for Hamiltonian simulation, achieving optimal asymptotic scaling in some or all parameters [Ber+15; LC16; Ber+14]. However, these algorithms all require substantial overhead both in number of qubits, and in large constant factors hidden in the big-O expressions for the asymptotic scaling. Recently, Childs and Su have shown that previous error bounds on Trotter product formulae were over-pessimistic. They derived new bounds showing that the older, simpler, product-formula algorithms achieve the same asymptotic scaling as the more sophisticated algorithms. For near-term hardware, achieving good asymptotic scaling is almost irrelevant; what matters is minimising the actual circuit depth or run-time for the particular target system being simulated. For the size of quantum many-body system accessible to near-term hardware (and possibly even for larger quantum hardware), simpler algorithms with low overhead are likely to be significantly better than more sophisticated algorithms with much larger constant factors. Furthermore, product-formula algorithms promise better control of error propagation in the absence of active error-correction and fault-tolerance, as explained in Section 1.1. Whereas the more sophisticated algorithms do not benefit from this.

For these reasons, we choose to implement the time evolution operator $U(T) := \exp(iTH)$ by employing Trotter product formulae $U(T) =: \mathcal{P}_p(\delta)^{T/\delta} + \mathcal{R}_p(T, \delta)$. Here, $\mathcal{R}_p(T, \delta)$ denotes the error term remaining from the approximate decomposition into a product of individual terms, defined directly as $\mathcal{R}_p(T, \delta) := U(T) - \mathcal{P}_p(\delta)^{T/\delta}$. This includes the simple first-order formula [Llo96]

$$\mathcal{P}_1(\delta)^{T/\delta} := \prod_{n=1}^{T/\delta} \prod_{i=1}^M e^{-iH_i\delta},$$

as well as higher-order variants [Suz92; Suz91; CS19]

$$\mathcal{P}_2(\delta) := \prod_{j=1}^M e^{-iH_j \delta/2} \prod_{j=M}^1 e^{-iH_j \delta/2},$$

$$\mathcal{P}_{2k}(\delta) := \mathcal{P}_{2k-2}(a_k \delta)^2 \mathcal{P}_{2k-2}((1 - 4a_k)\delta) \mathcal{P}_{2k-2}(a_k \delta)^2$$

for $k \in \mathbb{N}$, where the coefficients are given by $a_k := 1/(4 - 4^{1/(2k-1)})$. It is easy to see that, while for higher-order formulas not all pulse times equal δ , they still asymptotically scale as $\Theta(\delta)$. The product formula $\mathcal{P}_p(\delta)^{T/\delta}$ then approximates a time-evolution under $U(\delta)^{T/\delta} = U(T)$, and it describes the sequence of local unitaries to be implemented as a quantum circuit.

Choosing the Trotter step δ small means that corrections for every factor in this formula come in at $\mathcal{O}(\delta^{p+1})$ for $p \in \{1, 2k : k \in \mathbb{N}\}$. Since we have to perform T/δ many rounds, the overall error scales roughly as $\mathcal{O}(T\delta^p)$. Yet this rough estimate is insufficient if we need to calculate the largest-possible δ for our Hamiltonian simulation.

Let Λ denotes the number of fermions present in the simulation, such that $\|H_i|_{\Lambda \text{ fermions}}\| \leq \Lambda$ as shown in Section 5. The Hamiltonian dynamics remains entirely within one fermion number sector, as H_{FH} commutes with the total fermion number operator. Let $M = 5$ denote the number of non-commuting Trotter layers, and set $\epsilon_p(T, \delta) := \|\mathcal{R}_p(T, \delta)\|$, and as shorthand $\epsilon_p(\delta) := \epsilon_p(\delta, \delta)$, so that $\epsilon_p(T, \delta) = T/\delta \times \epsilon_p(\delta)$.

To obtain a bound on $\mathcal{P}_p(\delta)$, we apply the variation of constants formula [Kna05, Th. 4.9] to $\mathcal{R}_p(\delta)$, with the condition that $\mathcal{P}_p(0) = \mathbb{1}$, which always holds. As in [CS19, sec. 3.2], for $\delta \geq 0$, we obtain

$$\mathcal{P}_p(\delta) = U(\delta) + \mathcal{R}_p(\delta) = e^{-i\delta H} + \int_0^\delta e^{-i(\delta-\tau)H} R_p(\tau) d\tau \quad (3)$$

where the integrand $R_p(\tau)$ is defined as

$$R_p(\tau) := \frac{d}{d\tau} \mathcal{P}_p(\tau) - (-iH) \mathcal{P}_p(\tau).$$

Now, if $\mathcal{P}_p(\delta)$ is accurate up to p^{th} order – meaning that $\mathcal{R}_p(\delta) = \mathcal{O}(\delta^{p+1})$ – it holds that the integrand $R_p(\delta) = \mathcal{O}(\delta^p)$. This allows us to restrict its partial derivatives for all $0 \leq j \leq p-1$ to $\partial_\tau^j R_p(0) = 0$. For full details see Lemma 11 and [CS19, Order Conditions].

Then, following [CS19], we perform a Taylor expansion of $R_p(\tau)$ around $\tau = 0$, simplifying the error bound $\epsilon_p(\delta) \equiv \|\mathcal{R}_p(\delta)\|$ to

$$\begin{aligned} \epsilon_p(\delta) &= \left\| \int_0^\delta e^{-i(\delta-\tau)H} R_p(\tau) d\tau \right\| \leq \int_0^\delta \|R_p(\tau)\| d\tau \\ &= \int_0^\delta \left(\|R_p(0)\| + \|R_p'(0)\|\tau + \dots + \|R_p^{(p-1)}(0)\| \frac{\tau^{p-1}}{(p-1)!} + \|S_p(\tau, 0)\| \right) d\tau. \end{aligned}$$

Here we use the aforementioned order condition that for all $0 \leq j \leq p-1$ the partial derivatives satisfy $\partial_\tau^j R_p(0) = 0$, leaving all but the p^{th} or higher remainder terms $S_p(\tau, 0)$ equal to zero. Thus

$$\epsilon_p(\delta) \leq \int_0^\delta \|S_p(\tau, 0)\| d\tau = p \int_0^\delta \int_0^1 (1-x)^{p-1} \|R_p^{(p)}(x\tau)\| \frac{\tau^p}{p!} dx d\tau, \quad (4)$$

where we used the integral representation for the Taylor remainder $S_p(\tau, 0)$.

Motivated by this, we look for simple bounds on the p^{th} derivative of the integrand $\|R_p(\tau)\|$. At this point our work diverges from [CS19] by focusing on obtaining bounds on $\|R_p(\tau)\|$ which have the tightest constants for NISQ-era system sizes, but which now are *not* optimal in system size, see Fig. 8 and Lemmas 12 and 17 in Section 3 for details. We derive the following explicit error bounds (see Theorem 13 and Corollary 14 in Section 3):

$$\epsilon_p(\delta) \leq \delta^{p+1} M^{p+1} \Lambda^{p+1} \times \begin{cases} 1 & p = 1 \\ \frac{2}{(p+1)!} \left(\frac{10}{3}\right)^{(p+1)(p/2-1)} & p = 2k, k \geq 1, \end{cases} \quad (5)$$

$$\epsilon_p(\delta) \leq \frac{2\delta^{p+1} M^{p+1} \Lambda^{p+1}}{(p+1)!} H_p^{p+1} \quad \text{where} \quad H_p := \prod_{i=1}^{p/2-1} \frac{4 + 4^{1/(2i+1)}}{|4 - 4^{1/(2i+1)}|}. \quad (6)$$

The above expressions hold for generic Trotter formulae. Using Lemma 17 we can exploit commutation relations for the specific Hamiltonian at hand (whose structure determines N and n , see Section 4.5). This yields the bound (see Theorem 18):

$$\epsilon_p(\delta) \leq C_1 \frac{T\delta^p}{(p+1)!} + C_2 \frac{T}{\delta} \int_0^\delta p \int_0^1 (1-x)^{p-1} \frac{x\tau^{p+1}}{p!} e^{x\tau N B_p} dx d\tau \quad (7)$$

where

$$C_1 := npB_p^2 \Lambda^{p-1} N \left(MH_p - B_p + B_p \left(\frac{N}{\Lambda} \right) \right)^{p-1} \left((S_p M)^2 - (S_p M) \right) \quad (8)$$

$$C_2 := nB_p^2 (MH_p \Lambda)^p N \left((S_p M)^2 - (S_p M) \right). \quad (9)$$

$$B_p := \begin{cases} 1 & p = 1 \\ \frac{1}{2} & p = 2 \\ \frac{1}{2} \prod_{i=2}^k (1 - 4a_i) & p = 2k, k \geq 2. \end{cases} \quad (10)$$

These analytic error bounds are then combined with a Taylor-of-Taylor method, by which we expand the Taylor coefficient $R_p^{(p)}$ in Eq. (4) itself in terms of a power series to some higher order $q > p$, with corresponding series coefficients $R_p^{(q)}$, and a corresponding remainder-of-remainder error term $\epsilon_{p,q+1}$. The tightest error expression we obtain is (see Corollary 20 in Section 4.6):

$$\epsilon_p(\delta) \leq \sum_{l=p}^q \frac{\delta^{l+1} \Lambda^{l+1}}{(l+1)!} f(p, M, l) + \epsilon_{p,q+1}(\delta), \quad (11)$$

where the $f(p, M, l)$ are exactly-calculated coefficients (using a computer algebra package) that exploit cancellations in between the M non-commuting Trotter layers, for a product formula of order p and series expansion order l (given in Table 2). The series' remainder $\epsilon_{p,q+1}$ therein is then derived from the analytic bounds in Eq. (7) (see Section 4.3 for technical details).

Henceforth, in the subsequent discussion, we will assume the tightest choice of $\epsilon_p(\delta)$ amongst all the derived error expressions and choice of $p \in \{1, 2, 4\}$. In order to guarantee a target error bound such as $\epsilon_p(T, \delta) \leq \epsilon_t = 10\%$, we invert these explicitly derived error bounds and obtain a maximum possible Trotter step $\delta_0 = \delta_0(\epsilon_t)$.

1.4 Sub-Circuit-Model Synthesis of Trotter Layers

The Trotter product formula $\mathcal{P}_p(T, \delta)$ comprises local unitaries, corresponding to the local interaction terms that make up the five layers of Hamiltonians that we decomposed the Fermi Hubbard Hamiltonian into.

In order to implement each step of the product formula as a sequence of gates, we would ideally simply execute all two-, three- (for the LW encoding), or four-local (for the VC encoding) interactions necessary for the time evolution directly within the quantum computer. Yet this is an unrealistic assumption, as the quantum device is more likely to feature a very restricted set of one- and two-qubit interactions.

As outlined in Section 1.1, we assume in our model that arbitrary single qubit unitaries are available, and that we have access to the continuous family of gates $\exp(itZ \otimes Z)$ for arbitrary values of t . In contrast, the gates we wish to implement all have the form $\exp(i\delta Z^{\otimes k})$ for $k = 3$ or 4. (Or different products of k Pauli operators, but these are all equivalent up to local unitaries, which we are assuming are available.)

It is well known that a unitary describing the evolution under any k -local Pauli interaction can be straightforwardly decomposed into CNOT gates and single qubit rotations [NC10, Sec. 4.7.3]. For instance, we can decompose evolution under a 3-local Pauli as

$$e^{i\delta Z_1 Z_2 Z_3} = e^{-i\pi/4 Z_1 X_2} e^{i\delta Y_2 Z_3} e^{i\pi/4 Y_2 Z_3}, \quad (12)$$

where we then further decompose the remaining 2-local evolutions in Eq. (12) using the exact same method as

$$e^{i\delta Y_2 Z_3} = e^{-i\pi/4 Y_2 X_3} e^{i\delta Y_3} e^{i\pi/4 Y_2 Z_3}. \quad (13)$$

This effectively corresponds to decomposing $e^{i\delta Z_1 Z_2 Z_3}$ into CNOT gates and single qubit rotations, as $e^{\pm i\pi/4 Z_i Z_j}$ is equivalent to a CNOT gate up to single qubit rotations. To generate evolution under any k -local Pauli interaction we can simply iterate this procedure, which yields a constant overhead $\propto 2(k-1) \times \pi/4$.

Can we do better? Even optimized variants of Solovay-Kitaev to decompose multi-qubit gates – beyond introducing an additional error – generally yield gate sequences multiple orders of

magnitude larger, as e.g. demonstrated in [PVH13]. While more recent results conjecture that an arbitrary three-qubit gate can be implemented with at most eight $O(1)$ two-local entangling gates [Mar+16], this is still worse than the conjugation method for the particular case of a rank one Pauli interaction that we are concerned with.

For small pulse times δ , the existing decompositions are thus inadequate, as they all introduce a gate cost $\Omega(1) + O(\delta)$. In this paper, we develop a series of analytic pulse sequence identities (see Lemmas 6 and 7 in Section 3), which allow us to decompose the three-qubit and four-qubit gates as approximately ^{2 3}

$$e^{i\delta Z_1 Z_2 Z_3} \approx e^{-i\sqrt{\delta/2} Z_1 X_2} e^{i\sqrt{\delta/2} Y_2 Z_3} e^{i\sqrt{\delta/2} Z_1 X_2} e^{-i\sqrt{\delta/2} Y_2 Z_3}, \quad (14)$$

$$e^{i\delta Z_1 Z_2 Z_3 Z_4} \approx e^{-i0.22\delta^{2/3} Y_2 Z_3 Z_4} e^{-i1.13\delta^{1/3} Z_1 X_2} e^{i0.44\delta^{2/3} Y_2 Z_3 Z_4} e^{i1.13\delta^{1/3} Z_1 X_2} e^{-i0.22\delta^{2/3} Y_2 Z_3 Z_4}. \quad (15)$$

In reality we use the exact versions of these decompositions, which we also note are still exact for $\delta \geq 1$. The depth-5 decomposition in Eq. (15) yields the shortest overall time cost when breaking down higher-weight interactions in a recursive fashion, assuming that the remaining 3-local gates in are decomposed using an expression similar to Eq. (14). We also carry out numerical studies that indicate that these decompositions are likely to be optimal. (See Section 3.3 for details.) These circuit decompositions allow us to establish that, for a weight- k interaction term, there exists a pulse sequence which implements the evolution operator for time δ with an overhead $\propto \delta^{1/(k-1)}$, achieved by recursively applying these decompositions.⁴

For the interactions require for our Fermi-Hubbard simulation, the overhead of decomposing short-pulse gates with this analytic decomposition is $\propto \sqrt{\delta}$ for any weight-3 interaction term, and $\propto \delta^{1/3}$ for weight-4. The asymptotic time cost is thus $O(T\delta_0^w)$ for $w = -1/2$ (LW encoding) or $w = -2/3$ (VC encoding). We show the exact scaling for $k = 3$ and $k = 4$ in Fig. 3, as compared to the standard conjugation method.

1.5 Benchmarking the Sub-Circuit-Model

How significant is the improvement of all the measures set out in previous sections, as benchmarked against state-of-the-art results from literature? A first comparison is in terms of exact asymptotic

²The approximations in Eqs. (14) and (15) are shown to first order in δ . Exact analytic expressions, which also hold for $\delta \geq 1$, are derived in Section 3.

³The constants in Eq. (15) have been rounded to the third significant figure.

⁴While we have only made reference to interactions of the form $Z^{\otimes k}$, we remark that this is sufficient as we can obtain any other interaction term of the same weight, for example ZZZ , by conjugating $Z^{\otimes k}$ by single qubit rotations, H and SHS^\dagger in this example (where H is a Hadamard and S a phase gate).

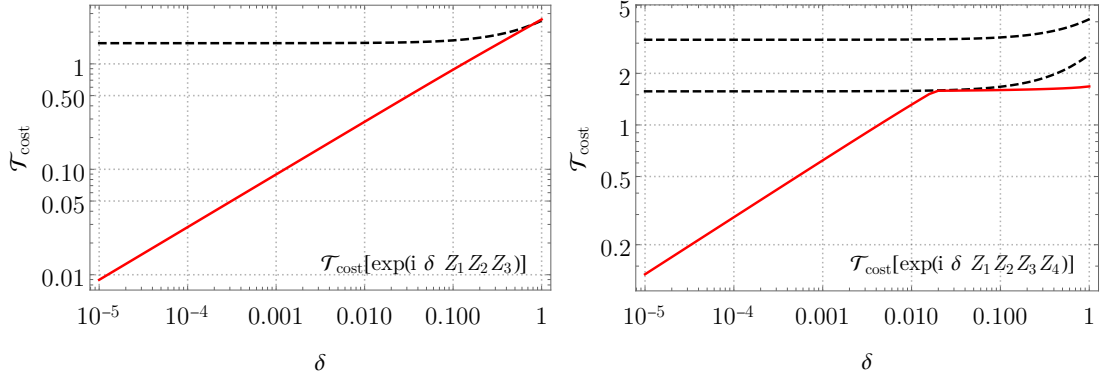


Figure 3: Gate decomposition overhead for decomposing $\exp(i\delta Z^{\otimes 3})$ (left) and $\exp(i\delta Z^{\otimes 4})$ (right), for $\delta \in [10^{-5}, 1]$. The lower dashed line is the cost obtained by conjugation decomposition, $\pi/2 + \delta$. The upper dashed line is the cost for a once-nested conjugation, $\pi + \delta$. Decomposing the four-local gate with an outer depth-5 and an inner depth-4 formula according to Eqs. (14) and (15) only saturates the lower conjugation cost bound.

bounds (which we derive in Remarks 23 and 24), in terms of the number of non-commuting Trotter layers M , fermion number Λ , simulation time T and target error ϵ_{target} :

$$\begin{aligned} \text{standard circuit model: } \mathcal{T}_{\text{cost}}(\mathcal{P}_p(\delta)^{T/\delta}) &= O\left(M^{2+1/p} \Lambda^{1+1/p} T^{1+1/p} \epsilon_{\text{target}}^{-1/p}\right), \\ \text{sub-circuit model: } \mathcal{T}_{\text{cost}}(\mathcal{P}_p(\delta)^{T/\delta}) &= O\left(M^{3/2+1/(2p)} \Lambda^{1/2+1/(2p)} T^{1+1/(2p)} \epsilon_{\text{target}}^{-1/(2p)}\right), \end{aligned}$$

where we write $\mathcal{T}_{\text{cost}}$ for the “wall time” of the quantum circuits – i.e. the sum of pulse times of all gates within the circuit. (See Definition 2 in Section 2 for a detailed discussion of the cost model we employ.)

Beyond asymptotic scaling, and in order to establish a more comprehensive benchmark that takes into account potentially large but hidden constant factors, we employ our tighter Trotter error bounds that account for all constant factors, and concretely target a 5×5 Fermi-Hubbard Hamiltonian for overall simulation time $T = 7$ (which is roughly the Lieb-Robinson time required for the “causality-cone” to spread across the whole lattice, and for correlations to potentially build up between any pair of sites), in the sector of $\Lambda = 5$ fermions, and coupling strengths $|u|, |v| \leq r = 1$ as given in Eq. (2). For this system, we choose the optimal Trotter product formula order p that yields the lowest overall time cost, while still achieving a target error of $\epsilon_{\text{target}} = 0.1$.

The results are given in Table 1, where we emphasize that in order to maintain a fair comparison, we always employ the same sub-circuit cost metric throughout: single-qubit gates are assumed a free resource,⁵ and time-cost of two-qubit gates is accounted at their pulse length.

⁵This is a reasonable simplified cost model for many quantum hardware devices, as single-qubit gates are typically an order of magnitude faster and an order of magnitude higher-fidelity than the two-qubit gates [Goo+19a; MN17].

Our newly-derived Trotter error bounds yield an order-of-magnitude improvement as compared to [Chi+17, Prop F.4]. And even for existing gate decompositions by conjugation, the novel lower-weight LW encoding yields a small but significant improvement. The most striking advantage comes from utilizing the sub-circuit sequence decompositions developed in this paper, in particular in conjunction with the lower-weight LW fermionic encoding.

Overall, the combination of new Trotter error bounds, low-weight fermion encoding and sub-circuit-model algorithm design, allows us to improve the run-time of the simulation algorithm from 800,160, to 2,960 – an improvement of more than three orders of magnitude over that obtainable using the previous state-of-the-art methods, and an even larger improvement over results in the preexisting literature [Kiv+19].

1.6 Sub-Circuit Algorithms on Noisy Hardware

As ours is a proposal for quantum simulation on near-term hardware we cannot neglect decoherence errors that inevitably occur throughout the simulation. To address this concern, we assume an iid noise model described by the qubit depolarizing channel

$$\mathcal{N}_q(\rho) = (1 - q)\rho + \frac{q}{3}(X\rho X + Y\rho Y + Z\rho Z) \quad (16)$$

applied to each individual qubit in the circuit, and after each gate layer in the Trotter product formula, and such that the bit, phase, and combined bit-phase-flip probability q is proportional to the elapsed time of the preceding layer. Whilst this standard error model is simplistic, it is a surprisingly good match to the errors seen in some hardware [Goo+19a].

Within this setting, a simple analytic decoherence error bound can readily be derived (see Section 6.5), by calculating the probability that zero errors appear throughout the circuit. If V denotes the *volume* of the circuit (defined as $\mathcal{T}_{\text{cost}} \times L^2$), then the depolarizing noise parameter $q < 1 - (1 - \epsilon_{\text{target}})^{1/V}$ – i.e. it needs to shrink exponentially quickly with the circuit’s volume. We emphasize that this is likely a crude overestimate. As outlined in Section 1.1, one of the major advantages of sub-circuit circuits is that, under a short-pulse gate, an error is only weakly propagated due to the reduced Lieb-Robinson velocity (discussed further in [Bau+20c]).

Yet irrespective of this overestimate, can we derive a tighter error bound by other means? In [Bau+20b], the authors analyse how noise on the physical qubits translates to errors in the fermionic code space. To first order and in the LW encoding, all of $\{X, Y, Z\}$ errors on the face, and $\{X, Y\}$ on the vertex qubits can be detected. Z errors on the vertex qubits result in an undetectable error, as evident from the form of $h_{\text{on-site}}$ from Eq. (39). It is shown in [Bau+20b, Sec. 3.2] that this Z error corresponds to fermionic phase noise in the simulated Fermi-Hubbard model.

It is therefore a natural extension to the notion of simulation to allow for *some* errors to occur, if they correspond to physical noise in the fermionic space. And indeed, as discussed more extensively in [Bau+20b, Sec. 2.4], phase noise is a natural setting for many fermionic condensed

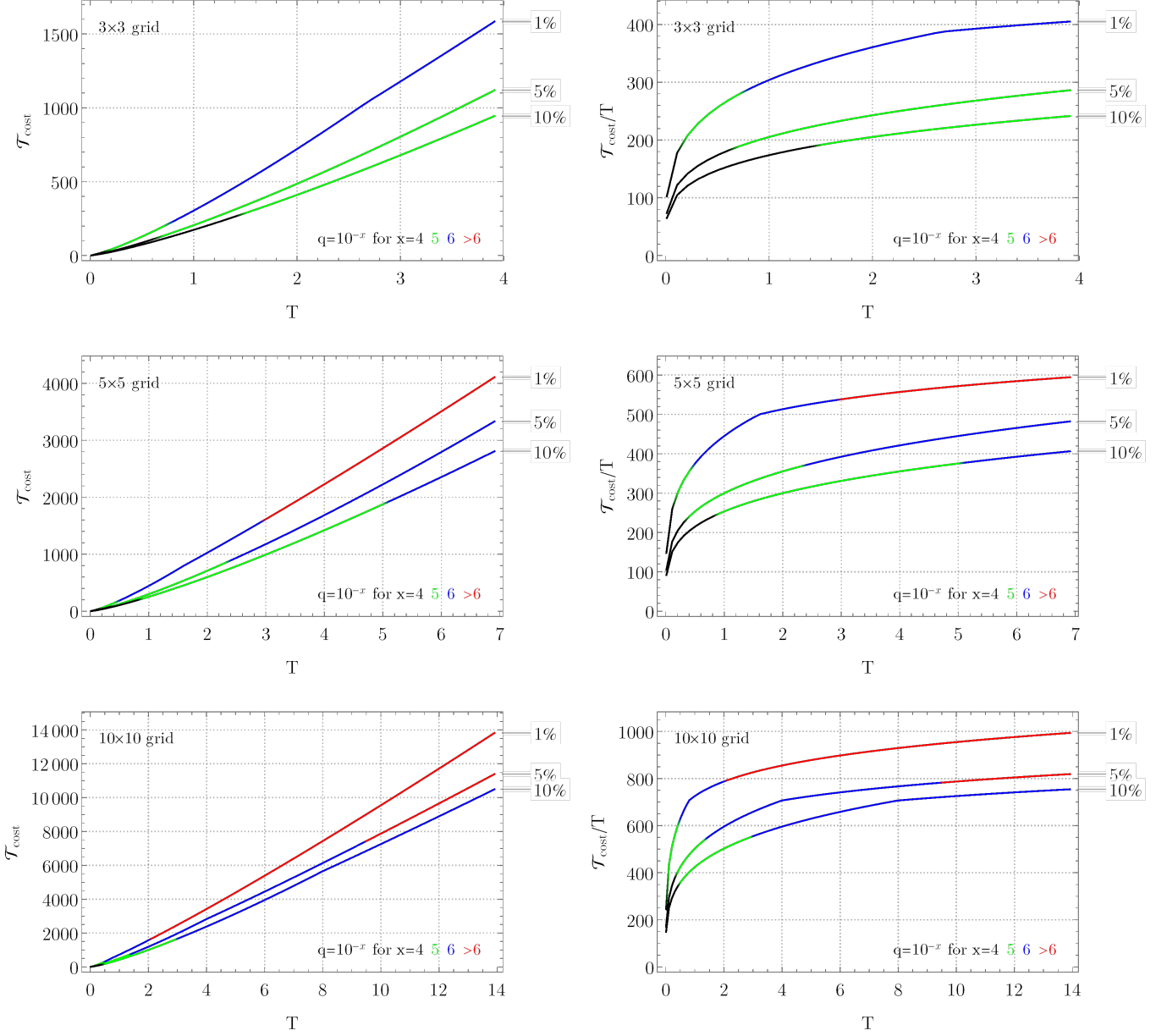


Figure 4: $\mathcal{T}_{\text{cost}}$ vs target time T (left) and overhead $\mathcal{T}_{\text{cost}}/T$ vs T (right), for lattice sizes 3×3 , 5×5 , and 10×10 , for the Fermi-Hubbard Hamiltonian H_{FH} from Eq. (38) in the LW encoding. In each plot, three lines represent 1%, 5%, and 10% Trotter error ϵ given in Eq. (27) (we use the tightest error expression from Corollaries 14 and 20 and Theorem 18), where we minimize over the product formula order $p \in \{1, 2, 4\}$ – higher p yielded worse cost for the plotted regimes. The line color corresponds to the intervals wherein the decoherence error of the circuit is upper-bounded by the Trotter error of the simulation, given a specific depolarizing noise parameter q . E.g. the blue section of the lower line means that the decoherence error remains below 10%, for $q = 10^{-6}$.

matter systems coupled to a phonon bath [Ng15; Kau+20; Zha+17; MF16; OT05; FF04; SD93] and [Rib14, Ch. 6.1&eq. 6.17].

How can we exploit the encoding’s error mapping properties? Under the assumption that X , Y and Z errors occur uniformly across all qubits, as assumed in Eq. (16), each Pauli error occurs with probability $q/3$. We further assume that we can measure all stabilizers (including a global parity operator) *once at the end of the entire circuit*, which can be done by dovetailing a negligible depth 4 circuit to the end of our simulation (see Section 6.6 for more details). We then numerically simulate a stochastic noise model for the circuit derived from aforementioned Trotter formula for a specific target error ϵ_{target} , for a Fermi-Hubbard Hamiltonian on an $L \times L$ lattice for $L \in \{3, 5, 10\}$.

Whenever an error occurs, we keep track of the syndrome violations they induce (including potential cancellations that happen with previous syndromes), using results from [Bau+20b] on how Pauli errors translate to error syndromes with respect to the fermion encoding’s stabilizers (summarized in Table 3). We then bin the resulting circuit runs into the following categories:

1. *detectable error*: at least one syndrome remains triggered, even though some may have canceled throughout the simulation,
2. *undetectable phase noise*: no syndrome was ever violated, and the only errors are Z errors on the vertex qubits which map to fermionic phase noise, and
3. *undetectable non-phase noise*: syndromes were at some point violated, but they all canceled.

This categorization allows us to calculate the maximum depolarizing noise parameter q to be able to run a simulation for time $T = \lfloor \sqrt{2}L \rfloor$ with target Trotter error $\epsilon_t \leq \epsilon_{\text{target}} \in \{1\%, 5\%, 10\%\}$, where we allow the resulting *undetectable non-phase noise* errors to also saturate this error bound, i.e. $\epsilon_s \leq \epsilon_{\text{target}}$. The overall error is thus guaranteed to stay below a propagated error probability of $(\epsilon_t^2 + \epsilon_s^2)^{1/2} \in \{1.5\%, 7.1\%, 15\%\}$, respectively.

In order to achieve these decoherence error bounds, one needs to postselect “good” runs and discard ones where errors have occurred, as determined from the single final measurement of all stabilizers of the LW encoding. The required overhead due to the postselected runs is mild, and shown in Fig. 19.

We plot the resulting simulation cost vs. target simulation time in Fig. 4, where we color the graphs according to the depolarizing noise rate required to achieve the target error bound. For instance, a depolarizing noise parameter $q = 10^{-4}$ allows simulating a 3×3 FH Hamiltonian for time $T \approx 1.5$, while satisfying a 15% error bound; the required circuit-depth-equivalent is $\mathcal{T}_{\text{cost}} \approx 200$. By contrast, a noise parameter $q = 10^{-6}$ suffices to simulate a 3×3 grid at 1.5%, a 5×5 grid at 7.1%, and a 10×10 grid at 15% error up to target simulation times $T = 4, 7$ and 14 , respectively.

1.7 Conclusions

In this work, we have derived a new method for designing quantum algorithms “one level below” the circuit model, by designing analytic sub-circuit identities to decompose the algorithm into. As a concrete example, we applied these techniques to the task of simulating time-dynamics of the spin Fermi-Hubbard Hamiltonian on a square lattice. Together with new Trotter product formulae error bounds, and a novel low-weight fermionic encoding, this improves upon state-of-the-art results by over three orders of magnitude in circuit-depth-equivalent. Childs et al. have recently extended their work on error bounds in [Chi+19], beyond their results in [CS19]. We have not yet incorporated their new bounds into our analysis, and this may give further improvements.

It is conceivable that other algorithms that require small unitary rotations will benefit from designing the implementations “bottom-up” instead of “top-down”. Standard circuit decompositions of many interesting quantum algorithms will remain unfeasible on real hardware for some time to come. Whereas our new sub-circuit-model algorithms, with their shorter overall run-time requirements and lower error-propagation even in the absence of error correction, potentially bring these algorithms and applications within reach of near-term NISQ hardware.

2 Sub-Circuit-Model and Cost Model

In this section we introduce the sub-circuit model, which we employ throughout this paper.

Definition 1 (Sub-circuit Model). *Given a set of qubits Q , a set $I \subseteq Q \times Q$ specifying which pairs of qubits may interact, a fixed two qubit interaction Hamiltonian h , and a minimum switching time t_{\min} , a sub-circuit pulse-sequence C is a quantum circuit of L pairs of alternating layer types $C = \prod_l U_l V_l$ with $U_l = \prod_{i \in Q} u_i^l$ being a layer of arbitrary single qubit unitary gates, and $V_l = \prod_{ij \in \Gamma_l} v_{ij} \left(t_{ij}^l \right)$ being a layer of non-overlapping, variable time, two-qubit unitary gates:*

$$v_{ij}(t) = e^{ith_{ij}}$$

with the set $\Gamma_l \subseteq I$ containing no overlapping pairs of qubits, and $t \geq t_{\min}$. Throughout this paper we assume $h_{ij} = Z_i Z_j$. As all $\sigma_i \sigma_j$ are equivalent to $Z_i Z_j$ up to single qubit rotations this can be left implicit and so we take $h_{ij} = \sigma_i \sigma_j$.

Unlike the traditional quantum circuit model which measures its time cost in layer count, the sub-circuit-model measures its time cost as the total physical duration of the two-qubit interaction layers.

Definition 2 (Sub-Circuit Physical Time Cost). *The physical time cost of a sub-circuit pulse-sequence C is defined as*

$$\mathcal{T}_{\text{cost}}(C) := \sum_l \max_{ij \in \Gamma_l} \left(t_{ij}^l \right)$$

The time cost is normalised to the physical interaction strength, so that $|h| = 1$. This cost model assumes that the single qubit layers contribute a negligible amount to the total time duration of the circuit.

This is justified for many implementations: for example superconducting qubits have interaction time scales of $\sim 50 - 500\text{ns}$ [Kja+19], while the single qubit energy spacing is on the order of $\sim 5\text{GHz}$, which gives a time scale for single qubit gates of $\sim 0.2\text{ns}$.

We can cost standard gates according to this definition as long as they are written in terms of a sub-circuit pulse-sequence. In this cost model a CNOT gate has $\mathcal{T}_{\text{cost}} = \pi/4$ as it is equivalent to $e^{-i\frac{\pi}{4}ZZ}$ up to single qubit rotations.

How does this cost model affect the time complexity of algorithms? I.e., given a circuit C , does $\mathcal{T}_{\text{cost}}(C)$ ever deviate so significantly from C 's gate depth count that the circuit would have to be placed in a complexity class lower? Under reasonable assumptions on the shortest pulse time we prove in the following that this is not the case.

Remark 3. Let $\{C_x\}_{x \in \mathbb{N}}$ be a family of quantum circuits ingesting input of size x . Denote with $m(x)$ the circuit depth of C_x ; and let $\delta_0 = \delta_0(x) := \min_{l \in [L]} \max_{ij \in \Gamma_l} (\tau_{ij}^l)$ be the shortest layer time pulse present in the circuit C_x , according to Definition 2. Then if

$$\delta_0(x) = \begin{cases} O(1) \\ 1/\text{poly } x \\ 1/\exp(\text{poly } x) \end{cases} \implies m(x) = \mathcal{T}_{\text{cost}}(C) \times \begin{cases} O(1) \\ O(\text{poly } x) \\ O(\exp(\text{poly } x)) \end{cases}$$

Furthermore $\mathcal{T}_{\text{cost}}(C) = O(m(x))$.

Proof. Clear since $m(x) = O(\mathcal{T}_{\text{cost}}(C)/\delta_0(x))$. The second claim is trivial. \square

An immediate consequence of using the cost model metric and the overhead of counting gates from Remark 3 can be summarized as follows.

Corollary 4. Let $\epsilon > 0$. Any family of short-pulse circuits $\{C_x\}$ with $\delta_0(x) = O(1)$ can be approximated by a family of circuits $\{\tilde{C}_x\}$ made up of gates from a fixed universal gate set; and such that \tilde{C}_x approximates C_x in operator norm to precision ϵ in time $O(\log^4(\mathcal{T}_{\text{cost}}(C_x)/\epsilon))$.

Proof. By Remark 3, there are $m(x) = \mathcal{T}_{\text{cost}}(C) \times O(1)$ layers of gates in C ; now apply Solovay-Kitaev to compile it to a universal target gate set. \square

Indeed, we can take this further and show that complexity classes like BQP are invariant under an exchange of the two metrics “circuit depth” and “ $\mathcal{T}_{\text{cost}}$ ”; if e.g. $\delta_0(x) = 1/\text{poly } x$, then again invoking Solovay-Kitaev lets one upper-bound and approximate any circuit while only introducing an at most polylogarithmic overhead in circuit depth. However, a stronger result than this is already known, independent of any lower bound on pulse times, which we cite here for completeness.

Remark 5 (Poulin et al. ([Pou+11])). A computational model based on simulating a local Hamiltonian with arbitrarily-quickly varying local terms is equivalent to the standard circuit model.

3 Decomposing Local Trotter Steps

3.1 Analytic Pulse Sequence Identities

In this section we introduce the analytic pulse sequence identities we use to decompose local Trotter steps $e^{-i\delta h}$. Their recursive application allows us to establish, that for a k -qubit Pauli interaction h , there exists sub-circuit pulse-sequence $C := \prod_l^L U_l V_l$ which implements the evolution operator $e^{-i\delta h}$. Most importantly, for any target time $\delta \geq 0$ the run-time of that circuit is bounded as

$$\mathcal{T}_{\text{cost}}(C) \leq O\left(\delta^{\frac{1}{k-1}}\right), \quad (17)$$

according to the notion of run-time established in Definition 2.

For $k = 2^n + 1$ where $n \in \mathbb{Z}$ as noted by [DBB07], this can be done inexactly using a well know identity from Lie algebra. For Hermitian operators A and B we have

$$e^{-itB}e^{-itA}e^{itB}e^{itA} = e^{t^2[A,B]} + O(t^3).$$

We make this exact for all $t \in [0, 2\pi]$ for anticommuting Pauli interactions in Lemma 6, and use Lemma 7 to extend it to all $k \in \mathbb{Z}$.

Lemma 6 (Depth 4 Decomposition). *Let $U(t) = e^{itH}$ be the time-evolution operator for time t under a Hamiltonian $H = \frac{1}{2i}[h_1, h_2]$, where h_1 and h_2 anti-commute and both square to identity. For $0 \leq \delta \leq \pi/2$ or $\pi \leq \delta \leq 3\pi/2$, $U(t)$ can be decomposed as*

$$U(t) = e^{it_1 h_1} e^{it_2 h_2} e^{it_2 h_1} e^{it_1 h_2} \quad (18)$$

with pulse times t_1, t_2 given by

$$\begin{aligned} t_1 &= \frac{1}{2} \tan^{-1} \left(\frac{1}{\sin(t) + \cos(t)}, \pm \frac{\sqrt{\sin(2t)}}{\sin(t) + \cos(t)} \right) + \pi c \\ t_2 &= \frac{1}{2} \tan^{-1} \left(\cos(t) - \sin(t), \mp \sqrt{\sin(2t)} \right) + \pi c, \end{aligned}$$

where $c \in \mathbb{Z}$, and corresponding signs are taken in the two expressions.

For $\pi/2 \leq t \leq \pi$ or $3\pi/2 \leq t \leq 2\pi$, $U(t)$ can be decomposed as

$$U(t) = e^{it_1 h_1} e^{it_2 h_2} e^{-it_2 h_1} e^{-it_1 h_2} \quad (19)$$

with pulse times t_1, t_2 given by

$$\begin{aligned} t_1 &= \frac{1}{2} \tan^{-1} \left(\frac{1}{\cos(t) - \sin(t)}, \pm \frac{\sqrt{-\sin(2t)}}{\cos(t) - \sin(t)} \right) + \pi c \\ t_2 &= \frac{1}{2} \tan^{-1} \left(\sin(t) + \cos(t), \pm \sqrt{-\sin(2t)} \right) + \pi c, \end{aligned}$$

where $c \in \mathbb{Z}$, and corresponding signs are taken in the two expressions.

Proof. Follows similarly to Lemma 25. □

Lemma 7 (Depth 5 Decomposition). *Let $U(t)$ be the time-evolution operator for time t under a Hamiltonian $H = \frac{1}{2i}[h_1, h_2]$. If h_1 and h_2 anti-commute and both square to identity, then $U(t)$ can be decomposed as*

$$U(t) = e^{it_1 h_2} e^{-i\phi h_1} e^{it_2 h_2} e^{i\phi h_1} e^{it_1 h_2} \quad (20)$$

with pulse times t_1, t_2, ϕ given by

$$t_1 = \frac{1}{2} \tan^{-1} \left(\pm \sqrt{2} \sec(t) \csc(2\phi) \sqrt{\cos(2t) - \cos(4\phi)}, -2 \tan(t) \cot(2\phi) \right) + \pi c$$

$$t_2 = \tan^{-1} \left(\pm \frac{\csc(2\phi) \sqrt{\cos(2t) - \cos(4\phi)}}{\sqrt{2}}, \sin(t) \csc(2\phi) \right) + 2\pi c$$

where $c \in \mathbb{Z}$, and corresponding signs are taken in the two expressions.

Proof. Follows similarly to Lemma 25. □

3.2 Pulse-Time Bounds on Analytic Decompositions

In our later analysis we apply these methods to the interactions in the Fermi-Hubbard Hamiltonian. Depending on the fermionic encoding used, these interaction terms are at most 3-local or 4-local. Fig. 5 depicts exactly how Lemmas 6 and 7 are used to decompose 3-local and 4-local interactions of the form $Z^{\otimes k}$.

We establish bounds on the run-time (Definition 2) of these circuits. The exact run-time of the circuit C_a – defined in Fig. 5a – follows directly from Definition 2 as

$$\mathcal{T}_{\text{cost}}(C_a(t)) = 2|t_1^a(t)| + 2|t_2^a(t)|.$$

We have labelled the functions $t_i(t)$ from Lemma 6 as $t_i^a(t)$ in order to distinguish them from those given in Lemma 7, which are now labelled $t_i^b(t)$. This is to avoid confusion when using both identities in the one circuit, such as in circuit C_b where we use Lemma 6 to decompose the remaining 3-local gates.

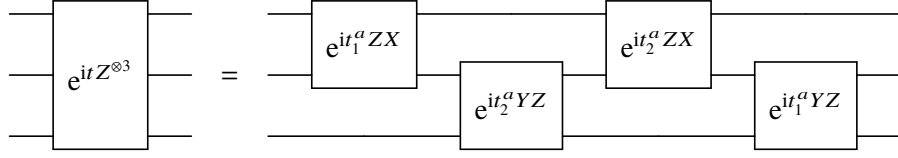
The exact run-time of the circuit C_b – defined in Fig. 5b – is left in terms of $\mathcal{T}_{\text{cost}}(C_a)$ and again follows directly from Definition 2 as

$$\mathcal{T}_{\text{cost}}(C_b(t, \phi)) = 2 \mathcal{T}_{\text{cost}}(C_a(t_1^b(t, \phi))) + \mathcal{T}_{\text{cost}}(C_a(t_2^b(t, \phi))) + 2|\phi|.$$

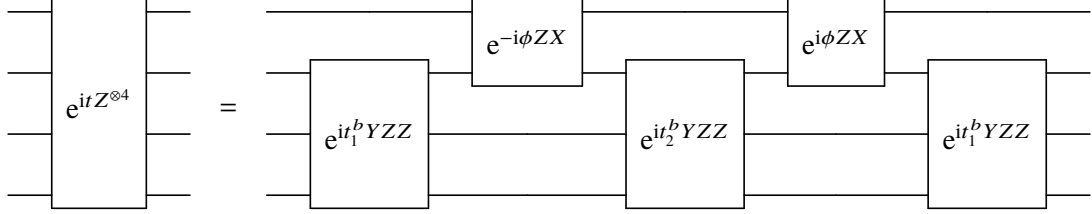
Lemmas 8 and 9 bound these two functions and determine the optimal choice of the free pulse-time ϕ . Inserting these bounds into the above $\mathcal{T}_{\text{cost}}$ expressions gives

$$\mathcal{T}_{\text{cost}}(C(t)) \leq \begin{cases} 2\sqrt{2}t & C = C_a \\ 7\sqrt[3]{t} & C = C_b \end{cases}. \quad (21)$$

As $Z^{\otimes k}$ is equivalent to any k -local Pauli term up to single qubit rotations, these bounds hold for any three or four local Pauli interactions.



(a) Circuit C_a . The pulse times $t_i^a(t)$ are defined in Lemma 6 and the run-time is bounded as $\mathcal{T}_{\text{cost}}(C_a(t)) \leq 2\sqrt{2}t$.



(b) Circuit C_b . The pulse times $t_i^b(t)$ are defined in Lemma 7. The three local gates are further decomposed using Lemma 6, though this is not shown here. If $\phi = \left(\frac{1}{4}(3 + 2\sqrt{2})t\right)^{1/3}$ then the run-time is bounded as $\mathcal{T}_{\text{cost}}(C_b(t)) \leq 7\sqrt[3]{t}$.

Figure 5: The definitions of circuits $C_a(t)$ and $C_b(t)$ – which respectively generate evolution under a three and four local Pauli interaction for target time $t \geq 0$.

Lemma 8. *Let H be as in Lemma 6. For $0 \leq t \leq \pi/2$, the pulse times t_i in Lemma 6 can be bounded by*

$$|t_1| \leq \sqrt{\frac{t}{2}}$$

$$|t_2| + |t_1| \leq \sqrt{2t}.$$

Proof. Choosing the negative $t_1(t)$ and corresponding $t_2(t)$ solution from Lemma 6 and Taylor expanding about $t = 0$ gives

$$t_1(t) = -\sqrt{\frac{t}{2}} + R_1(t)$$

$$t_2(t) = \sqrt{\frac{t}{2}} + R_2(t).$$

Basic calculus shows that t_1 is always negative and t_2 is always positive for $0 \leq t \leq \pi/2$, thus

$$|t_2| + |t_1| = t_2 - t_1 = \sqrt{2t} + R_{12}(t).$$

Then it can be shown that the Taylor remainders R_1 and R_{12} are positive and negative, respectively, giving the stated bounds. \square

Lemma 9. Let H be as in Lemma 7. For $0 \leq t \leq t_c$ and $\phi = (ct)^{1/3}$, the pulse times t_i in Lemma 7 can be bounded by

$$\begin{aligned} 2\sqrt{2|t_2|} + 4\sqrt{2|t_1|} + 2|\phi| &\leq 3(6 + 4\sqrt{2})^{1/3} t^{1/3} \\ &\leq 7t^{1/3}, \end{aligned}$$

where $c = \frac{1}{4}(3 + 2\sqrt{2})$ and $t_c \sim 0.33$.

Proof. This follows similarly to Lemma 8. We choose the positive branch of the \pm solutions for pulse times with $t_1(t)$ and $t_2(t)$ given in Lemma 7, and freely set $\phi = (ct)^{1/3}$ for some positive constant $c \in \mathbb{R}$. Within the range $0 \leq t \leq t_c$ we have real pulse times $t_1 \leq 0$ and $t_2 \geq 0$. We can then Taylor expand the following about $t = 0$ to find

$$\begin{aligned} 2\sqrt{2|t_2|} + 4\sqrt{2|t_1|} + 2|\phi| &= 2\sqrt{2t_2} + 4\sqrt{-2t_1} + 2(ct)^{1/3} \\ &= \frac{2(\sqrt{c} + \sqrt{2} + 1)}{\sqrt[3]{c}} t^{1/3} + R(t). \end{aligned}$$

Choosing c to minimise the first term in this expansion, and again showing that $R \leq 0$, leads to the stated result

$$\begin{aligned} 2\sqrt{2|t_2|} + 4\sqrt{2|t_1|} + 2|\phi| &\leq 3(6 + 4\sqrt{2})^{1/3} t^{1/3} \\ &\leq 7t^{1/3} \end{aligned}$$

where $\phi = (ct)^{1/3}$ and $c = \frac{1}{4}(3 + 2\sqrt{2})$. This is valid only with the region $0 \leq t \leq t_c$ where $t_c \approx 0.33$. \square

The depth 5 decomposition has an important feature. The free choice of ϕ allows us to avoid incurring a fixed root overhead with every iterative application of this decomposition. That is when using it to decompose any $e^{itZ^{\otimes k}}$, we can always choose h_1 as a 2-local interaction and h_2 as a $(k-1)$ -local interaction. We can choose $\phi \propto t^{\frac{1}{k-1}}$ and a similar analysis as above will show that this leaves the remaining pulse-times as $t_i \propto t^{1-\frac{1}{k-1}}$. This can be iterated to decompose the remaining gates, all of the form of evolution under $(k-1)$ -local interactions for times $\propto t^{1-\frac{1}{k-1}}$. At each iteration we choose to h_1 as a 2-local interaction and $\phi \propto t^{\frac{1}{k-1}}$. Hence after $k-2$ iterations we will have established the claim stated in Eq. (17).

3.3 Optimality

An obvious question to ask at this point is whether the proposed decompositions are optimal, in the sense that they minimise the total simulation time $\mathcal{T}_{\text{cost}}$ while reproducing the target gate h exactly. A closely related question is then whether relaxing the condition that we want to simulate the target gate without any error allows us to reduce the scaling of $\mathcal{T}_{\text{cost}}$ with regards to the target time δ .

In this section we perform a series of numerical studies which indicate that the exact decompositions described in this section are indeed optimal within some parameter bounds, and that relaxing the goal to approximate implementations gives no benefit.

The setup is precisely as outlined in Section 3: for $U_{\text{target}} = \exp(iTZ^{\otimes k})$ for some locality $k > 1$ and time $T > 0$, we iterate over all possible gate sequences of width k and length n , the set of which we call $U_{n,k}$. For each sequence $U \in U_{n,k}$, we perform a grid search over all parameter tuples $(t_1, \dots, t_n) \in [-\pi/2, \pi/2]^n$ and $\delta \in [0, \pi/10]$, and calculate the parameter tuple $(\epsilon(U), \mathcal{T}_{\text{cost}})$, where $\mathcal{T}_{\text{cost}}$ is given in Definition 2, and

$$\epsilon(U) := \|U - U_{\text{target}}\|_2.$$

The results are binned into brackets over $(\delta, \mathcal{T}_{\text{cost}}) \in [\pi/10, n\pi/2]$ and their minimum within each bracket is taken. This procedure yields two outcomes:

1. For each target time δ and each target error $\epsilon > 0$, it yields the smallest $\mathcal{T}_{\text{cost}}$, depth n circuit with error less than ϵ , and
2. for each target time δ and each $\mathcal{T}_{\text{cost}}$, the smallest error possible with any depth n gate decomposition and total pulse time less than $\mathcal{T}_{\text{cost}}$.

This algorithm scales exponentially both in k and n , and polynomial in the number of grid search subdivisions. The following optimizations were performed.

1. We remove duplicate gate sequences under permutations of the qubits (since U_{target} is permutation symmetric).
2. We restrict ourselves to two-local Pauli gates, since any one-local gate can always be absorbed by conjugations, and
3. We remove mirror-symmetric sequences (since Paulis are self-adjoint).
4. For $n > 4$ we switch to performing a random sampling algorithm instead of grid search, since the number of grid points becomes too large.

Results for $k = 3$ and $n = 3, 4, 5$ are plotted in Figs. 6 and 7.

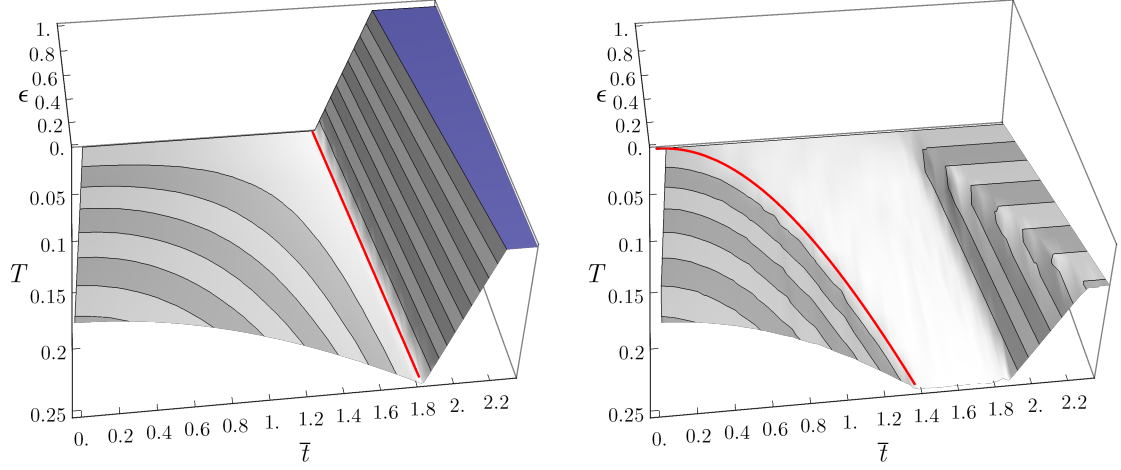


Figure 6: Numerical calculation of gate decomposition errors of the $U_{\text{target}} = \exp(iTZ^{\otimes 3})$ gate, with a pulse sequence of depth 3 (left) and depth 4 (right). Plotted in red are the optimal analytical decompositions given by CNOT conjugation and Lemma 6, respectively.

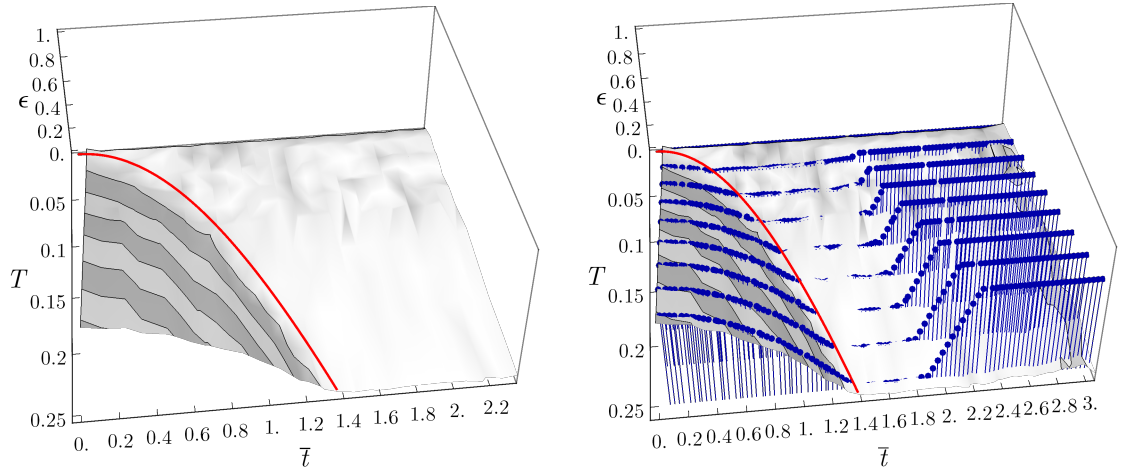


Figure 7: Numerical calculation of gate decomposition errors of the $U_{\text{target}} = \exp(iTZ^{\otimes 3})$ gate, with a pulse sequence of depth 5. Plotted in red is the optimal analytical decompositions given for a depth 4 sequence in Lemma 6; the blue lines are an overlay over the optimal depth 4 sequences from Fig. 6.

As can be seen (plotted as red line), for $n = 3$ the optimal zero-error decomposition has $\mathcal{T}_{\text{cost}} = \pi + \delta$ from CNOT conjugation. For $n = 4$, the optimal decomposition is given by the implicitly-defined solution in Lemma 6, with a $\mathcal{T}_{\text{cost}} \propto \sqrt{\delta}$ dependence. For the depth 5 sequences, it appears that the same optimality as for depth 4 holds. In contrast to $n = 3$ and $n = 4$, there is now a zero error solution for all $\mathcal{T}_{\text{cost}}$ greater than the optimum threshold.

4 Suzuki-Trotter Formulae Error Bounds

4.1 Existing Trotter Bounds

Trotter error bounds have seen a spate of dramatic and very exciting improvements in the past few years [Chi+17; CS19; Chi+19]. However, among these recent improvements we could not find a bound that was exactly suited to our purpose.

We wanted bounds which took into account the commutation relations between interactions in the Hamiltonian, as we know this leads to tighter error bounds [CS19] [Chi+17]. However, we needed exact constants in the error bound when applied to 2D lattice Hamiltonians, such as the 2D Fermi-Hubbard model. For this reason we could not directly apply the results of [CS19] which only explicitly obtains constants for 1D lattice Hamiltonians.

Additionally, we needed to be able to straightforwardly compute the bound for any higher order Trotter formula. This ruled out using the commutator bounds of [Chi+17] as they become difficult to compute at higher orders. Furthermore these bounds require each Trotter layer to consist of a single interaction, meaning we wouldn't be able to exploit the result of Section 5.

We followed the notation and adapted the methods of [CS19] to derive bounds that meet the above criteria. Additionally we incorporate our own novel methods to tighten our bounds in Corollaries 14 and 20 and Section 5.

The authors of [CS19] have recently extended their work further in [Chi+19]. We have not yet seen whether they will further tighten our analysis, though we are keen to do this in future work.

4.2 Hamiltonian Simulation by Trotterisation

In this section we derive our bounds for Trotter error. The standard approach to implementing time-evolution under a local Hamiltonian $H = \sum_i h_i$ on a quantum computer is to ‘‘Trotterise’’ the time evolution operator $U(T) = e^{-iHT}$. Assuming that the Hamiltonian breaks up into M mutually non-commuting layers $H = \sum_{i=1}^M H_i$ – i.e. such that $\forall i \neq j [H_i, H_j] \neq 0$ – Trotterizing in its basic form means expanding

$$U(T) := e^{-iHT} = \prod_{n=1}^{T/\delta} \prod_{i=1}^M e^{-iH_i\delta} + \mathcal{R}_1(T, \delta) = \mathcal{P}_1(\delta)^{T/\delta} + \mathcal{R}_1(T, \delta) \quad (22)$$

and then implementing the approximation $\mathcal{P}_1(\delta)^{T/\delta}$ as a quantum circuit. Here $\mathcal{R}_1(T, \delta)$ denotes the error term remaining from the approximate decomposition into a product of individual terms. $R_1(T, \delta) := U(T) - \mathcal{P}_1(\delta)^{T/\delta}$ is simply defined as the difference to the exact evolution $U(T)$. For M mutually non-commuting layers of interactions H_i , we must perform M sequential layers per Trotter step.

Eq. (22) is an example of a first-order product formula, and is derived from the Baker-Campbell-Hausdorff identity

$$e^{A+B} = e^A e^B e^{[A,B]/2} \dots \quad \text{and} \quad e^{A+B} = e^{(\delta A + \delta B)/\delta} = \left[e^{\delta A + \delta B} \right]^{1/\delta}.$$

Choosing δ small in Eq. (22) means that corrections for every factor in this formula come in at $O(\delta^2)$ i.e. in the form of a commutator, and since we have to perform $1/\delta$ many rounds of the sequence $e^{\delta A} e^{\delta B}$ the overall error scales roughly as $O(\delta)$.

Since its introduction in [Llo96], there have been a series of improvements, yielding higher-order expansions with more favourable error scaling. For a historical overview of the use of Suzuki-Trotter formulas in the context of Hamiltonian simulation, we direct the reader to the extensive overview given in [Yun+14, sec. 2.2.1]. In the following, we discuss the most recent developments for higher order product formulas, and analyse whether they yield an improved overall time and error scaling with respect to our introduced cost model in Section 2.

To obtain higher-order expansions, Suzuki derived an iterative expression for product formulas in [Suz92; Suz91]. For the $(2k)^{\text{th}}$ order, it reads [CS19]

$$\mathcal{P}_2(\delta) := \prod_{j=1}^M e^{-iH_j \delta/2} \prod_{j=M}^1 e^{-iH_j \delta/2}, \quad (23)$$

$$\mathcal{P}_{2k}(\delta) := \mathcal{P}_{2k-2}(a_k \delta)^2 \mathcal{P}_{2k-2}((1 - 4a_k)\delta) \mathcal{P}_{2k-2}(a_k \delta)^2, \quad (24)$$

where the coefficients are given by $a_k := 1/(4 - 4^{1/(2k-1)})$. The product limits indicate in which order the product is to be taken. The terms in the product run from right to left, as gates in a circuit would be applied, so that $\prod_{j=1}^L A_j = A_L \cdots A_1$.

4.3 Error Analysis of Higher-Order Formulae

We need an expression for the error $\mathcal{R}_p(T, \delta)$ arising from approximating the exact evolution $U(T)$ by a p^{th} order product formula $\mathcal{P}_p(\delta)$ repeated T/δ times. As a first step, we bring the latter into the form:

$$\mathcal{P}_p(\delta) := \prod_{j=1}^S \mathcal{P}_{p,j}(\delta) = \mathcal{P}_{p,S}(\delta) \cdots \mathcal{P}_{p,2}(\delta) \mathcal{P}_{p,1}(\delta), \quad (25)$$

$$\mathcal{P}_{p,j}(\delta) := \prod_{i=1}^M U_{ij}(\delta) \quad \text{where} \quad U_{ij}(\delta) := e^{-i\delta b_{ji} H_i}. \quad (26)$$

As before, M denotes the number of non-commuting *layers* of interactions in the local Hamiltonian. $S = S_p$ is the number of *stages*; the number of $\mathcal{P}_{p,j}(\delta)$ in a p^{th} order decomposition from Eq. (23) or Eq. (24). Here we note that we count a single stage as either $\prod_{i=1}^M U_{ij}(\delta)$ or $\prod_{i=M}^1 U_{ij}(\delta)$, so that a second order formula is composed of 2 stages.

Lemma 10. For a p^{th} -order decomposition with $p = 1$ or $p = 2k$, $k \geq 1$, we have $\sum_{j=1}^S b_{ji}(p) = 1$ for all $i = 1, \dots, M$. Furthermore, the Trotter coefficients b_{ji} satisfy

$$\max_{ij} \{|b_{ji}|\} \leq B_p \leq \begin{cases} 1 & p = 1 \\ \frac{1}{2} \left(\frac{2}{3}\right)^{k-1} & p = 2k, k \geq 1 \end{cases}$$

where

$$B_p := \begin{cases} 1 & p = 1 \\ \frac{1}{2} & p = 2 \\ \frac{1}{2} \prod_{i=2}^k (1 - 4a_i) & p = 2k, k \geq 2. \end{cases}$$

Proof. The first claim is obviously true for the first order formula in Eq. (22). For higher orders, by [CS19, Th. 3] and Eq. (22), we have that the first derivative

$$\left. \frac{\partial}{\partial x} \mathcal{P}_p(x) \right|_{x=0} = -i \sum_{i=1}^M H_i.$$

Similarly, from Eqs. (23) and (24), we have that

$$\left. \frac{\partial}{\partial x} \mathcal{P}_p(x) \right|_{x=0} = \frac{\partial}{\partial x} \prod_{j=1}^S \prod_{i=1}^M U_{ij}(x) \Big|_{x=0} = -i \sum_{j=1}^S \sum_{i=1}^M b_{ji} H_i.$$

Equating both expressions for the first derivative of $\mathcal{P}_p(x)$ at $x = 0$ and realising that they have to hold for any H_i yields the claim.

The second claim is again obviously true for a first order expansion, and follows immediately from Eq. (23) for $p = 2$. Expanding Eq. (24) for $\mathcal{P}_{2k}(\delta)$ all the way down to a product of \mathcal{P}_2 terms, the argument of each of the resulting factors will be a product of $k - 1$ terms of $a_{k'}$ or $1 - 4a_{k'}$ for $k' \leq k$. We further note that for $k \geq 2$, $|a_k| \leq |1 - 4a_k|$, as well as $|a_k| \leq 1/2$ and $|1 - 4a_k| \leq 2/3$, which can be shown easily. The b_{ji} can thus be upper-bounded by B_p , which in turn is upper-bounded by $(1/2)(2/3)^{k-1}$ – where the final factor of $(1/2)$ is obtained from the definition of \mathcal{P}_2 . \square

Since we are working with a fixed product formula order p for the remainder of this section, we will drop the order subscript in the following and write $\mathcal{P}_p = \mathcal{P}$, $\mathcal{R}_p = \mathcal{R}$ for simplicity. Assuming $\|H_i\| \leq \Lambda$ for all $i = 1, \dots, M$, and setting the error

$$\epsilon_p(T, \delta) := \|\mathcal{R}(T, \delta)\| = \|U(T) - \mathcal{P}(\delta)^{T/\delta}\|, \quad (27)$$

we can derive an expression for the p^{th} order error term. First, note that approximation errors in circuits accumulate at most linearly in Eq. (27). Thus it suffices to analyse a single δ step of the approximation, i.e. $U(\delta) = \mathcal{P}(\delta) + \mathcal{R}(\delta, \delta)$. Then

$$\epsilon_p(\delta) := \epsilon_p(\delta, \delta) = \|U(\delta) - \mathcal{P}(\delta)\| \quad (28)$$

so that

$$\epsilon_p(T, \delta) \leq \frac{T}{\delta} \epsilon_p(\delta). \quad (29)$$

We will denote $\epsilon_p(\delta)$ simply by ϵ in the following.

To obtain a bound on $\mathcal{P}(\delta)$, we apply the variation of constants formula with the condition that $\mathcal{P}(0) = \mathbb{1}$, which always holds. As in [CS19, sec. 3.2], for $\delta \geq 0$, we obtain

$$\mathcal{P}(\delta) = U(\delta) + \mathcal{R}(\delta) = e^{-i\delta H} + \int_0^\delta e^{-i(\delta-\tau)H} R(\tau) d\tau \quad (30)$$

where the integrand $R(\tau)$ is defined as

$$R(\tau) := \frac{d}{d\tau} \mathcal{P}(\tau) - (-iH) \mathcal{P}(\tau).$$

Now, if $\mathcal{P}(\delta)$ is accurate up to p^{th} order – meaning that $\mathcal{R}(\delta) = O(\delta^{p+1})$ – it holds that the integrand $R(\delta) = O(\delta^p)$. This allows us to restrict its partial derivatives, as the following shows.

Lemma 11. *For a product formula accurate up to p^{th} order – i.e. for which $R(\delta) = O(\delta^p)$ – the partial derivatives $\partial_\tau^j R(0) = 0$ for all $0 \leq j \leq p-1$.*

Proof. We note that $R(\delta)$ is analytic, which means that we can expand it as a Taylor series $R(\delta) = \sum_{j=0}^\infty a_j \delta^j$. We proceed by induction. If $a_0 \neq 0$, then clearly $R(0) \neq 0$, which contradicts the assumption that $R(\delta)$ is accurate up to p^{th} order. Now assume for induction that $\forall j < j' < p-1 : a_j = 0$ and $a_{j'} \neq 0$. Then

$$\frac{R(\delta)}{T^{j'}} = a_{j'} + \sum_{i=1}^\infty a_{i+j'} T^i \xrightarrow{\delta \rightarrow 0} a_{j'} \neq 0,$$

which again contradicts that $R(0) = O(\delta^p)$. The claim follows. \square

Performing a Taylor expansion of $R(\tau)$ around $\tau = 0$, the error bound ϵ given in Eq. (28) simplifies to

$$\epsilon = \left\| \int_0^\delta e^{-i(\delta-\tau)H} R(\tau) d\tau \right\| \leq \int_0^\delta \|R(\tau)\| d\tau \quad (31)$$

$$= \int_0^\delta \left(\|R(0)\| + \|R'(0)\| \tau + \dots + \|R^{(p-1)}(0)\| \frac{\tau^{p-1}}{(p-1)!} + \|S(\tau, 0)\| \right) d\tau, \quad (32)$$

Further by Lemma 11 all but the p^{th} or higher remainder terms $S(\tau, 0)$ equal zero, so

$$\epsilon \leq \int_0^\delta \|S(\tau, 0)\| d\tau = p \int_0^\delta \int_0^1 (1-x)^{p-1} \|R^{(p)}(x\tau)\| \frac{\tau^p}{p!} dx d\tau, \quad (33)$$

where we used the integral representation for the Taylor remainder $S(\tau, 0)$.

Motivated by this, we look for a simple expression for the p^{th} derivative of the integrand $R(\tau)$, which capture this in the following technical lemma.

Lemma 12. For a product formula accurate to p^{th} order, having $S = S_p$ stages for M non-commuting Hamiltonian layers with the upper-bound $\|H_i\| \leq \Lambda$, the error term $R(\tau)$ satisfies

$$\left\| \frac{\partial^p}{\partial \tau^p} R(\tau) \right\| \leq (SM)^{p+1} \Lambda^{p+1} \begin{cases} 2 & p = 1 \\ \frac{1}{2^p} \left(\frac{2}{3} \right)^{(p+1)(p/2-1)} & p = 2k \text{ for } k \geq 1. \end{cases}$$

Proof. We first express $\mathcal{P}(\tau)$ from Eqs. (25) and (26) with a joint index set $\Sigma = [S] \times [M]$ as

$$\mathcal{P}(\tau) = \prod_{j=1}^S \prod_{i=1}^M U_{ij}(\tau) = \prod_{I \in \Sigma} U_I(\tau).$$

Then the $(p+1)^{\text{th}}$ derivative of this with respect to τ is

$$\mathcal{P}^{(p+1)}(\tau) = \sum_{\alpha: |\alpha|=p+1} \binom{p+1}{\alpha} \prod_I U_I^{(\alpha_I)}(\tau) \quad (34)$$

where α is a multiindex on Σ , and $|\alpha| = \sum_{I \in \Sigma} \alpha_I$. Following standard convention, the multinomial coefficient for a multiindex is defined as

$$\binom{p+1}{\alpha} = \frac{(p+1)!}{\alpha!} = \frac{(p+1)!}{\prod_{I \in \Sigma} \alpha_I!}.$$

We can similarly express H with the same index set σ , and as a derivative of U via

$$H = \sum_{i=1}^S H_i = \sum_{j=1}^S \sum_{i=1}^M b_{ji} H_i = i \sum_{j=1}^S \sum_{i=1}^M U_{ij}^{(1)}(0) = i \sum_{I \in \Sigma} U_I^{(1)}(0) \quad (35)$$

where we used the fact that $\sum_{j=1}^S b_{ji} = 1$ by Lemma 10, and the exponential expression of U_I from Eq. (26).

Now we can combine Eqs. (34) and (35) as in Eq. (33) to obtain the p^{th} derivative of the integrand $R(\tau)$:

$$R^{(p)}(\tau) = \sum_{\alpha: |\alpha|=p+1} \binom{p+1}{\alpha} \prod_I U_I^{(\alpha_I)}(\tau) - \sum_I U_I^{(1)}(0) \sum_{\beta: |\beta|=p} \binom{p}{\beta} \prod_I U_I^{(\beta_I)}(\tau). \quad (36)$$

Noting that $\|U_I^{(\beta_I)}(\tau)\| = \|U_I^{(\beta_I)}(0)\|$, and further $U_I^{(x)}(0) U_I^{(y)}(0) = U_I^{(x+y)}(0)$, we have

$$\sum_J \|U_J^{(1)}(0)\| \sum_{\beta: |\beta|=p} \binom{p}{\beta} \prod_I \|U_I^{(\beta_I)}(0)\| = \sum_{\beta: |\beta|=p+1} \binom{p+1}{\beta} \prod_I \|U_I^{(\beta_I)}(0)\|.$$

We can therefore bound the norm of $R^{(p)}$ as follows:

$$\begin{aligned}
\|R^{(p)}(\tau)\| &\leq \sum_{\alpha: |\alpha|=p+1} \binom{p+1}{\alpha} \prod_I \|U_I^{(\alpha_I)}(0)\| \\
&\quad + \sum_I \|U_I^{(1)}(0)\| \sum_{\beta: |\beta|=p} \binom{p}{\beta} \prod_I \|U_I^{(\beta_I)}(0)\| \\
&= 2 \sum_{\alpha: |\alpha|=p+1} \binom{p+1}{\alpha} \prod_I \|U_I^{(\alpha_I)}(0)\| \\
&= 2 \sum_{\alpha: |\alpha|=p+1} \binom{p+1}{\alpha} \prod_{j=1}^S \prod_{i=1}^M |b_{ji}|^{\alpha_{ij}} \|H_i\|^{\alpha_{ij}}.
\end{aligned}$$

By Lemma 10, we know that $|b_{ji}| = 1$ when $p = 1$ and $|b_{ji}| \leq (2/3)^{p/2-1}/2$ for all j, i when $p = 2k$ for $k \geq 1$. Hence for $p = 1$

$$\|R^{(1)}(\tau)\| \leq 2(SM)^2 \Lambda^2,$$

and for $p = 2k$ for $k \geq 1$

$$\|R^{(p)}(\tau)\| \leq 2 \sum_{\alpha: |\alpha|=p+1} \binom{p+1}{\alpha} \left[\left(\frac{2}{3} \right)^{p/2-1} \frac{\Lambda}{2} \right]^{|\alpha|} =: C_p(S, M) \left(\frac{2}{3} \right)^{(p+1)(p/2-1)} \frac{\Lambda^{p+1}}{2^p},$$

where $C_p(S, M)$ is the sum of the multinomial coefficients of length $p \in \mathbb{N}$; a simple expression can be obtained by reversing the multinomial theorem, since

$$\sum_{\alpha: |\alpha|=p+1} \binom{p+1}{\alpha} = \left(\underbrace{1 + 1 + \dots + 1}_{|\Sigma| \text{ terms}} \right)^{p+1} = |\Sigma|^{p+1} = (SM)^{p+1}. \quad \square$$

To obtain the final error bounds, we combine Lemma 12 with the integral representation in Eq. (33).

Theorem 13 (Trotter Error). *For a p^{th} order product formula \mathcal{P}_p for $p = 1$ or $p = 2k$, $k \geq 1$, with the same setup as in Lemma 12, a bound on the approximation error for the exact evolution $U(T)$ with T/δ rounds of the product formula $\mathcal{P}_p(\delta)$ is given by*

$$\epsilon_p(T, \delta) \leq \frac{T}{\delta} \delta^{p+1} M^{p+1} \Lambda^{p+1} \times \begin{cases} 1 & p = 1 \\ \frac{2}{(p+1)!} \left(\frac{10}{3} \right)^{(p+1)(p/2-1)} & p = 2k, k \geq 1. \end{cases}$$

Proof. We can use the bound on $R^{(p)}$ derived in Lemma 12 and perform the integration over τ and x in Eq. (33), to obtain

$$\epsilon \leq \|R^{(p)}\| \int_0^\delta p \int_0^1 (1-x)^{p-1} \frac{\tau^p}{p!} dx d\tau = \frac{\delta^{p+1}}{(p+1)!} \|R^{(p)}\|.$$

By Lemma 11, for Trotter formulae of order $p = 1$ we have precisely one stage, i.e. $S = 1$, and $b_{ji} = 1$ for all i, j . This, together with Lemma 12 and Eq. (28), yields the first bound.

The number of stages in higher order formulae can be upper-bounded by Eqs. (23) and (24), giving $S_p \leq 2 \times 5^{p/2-1}$. Together with Lemma 12 and Eq. (28), this yields the second bound. \square

We remark that tighter bounds than the ones in Theorem 13 are achievable for any given product formula, where the form of its coefficients b_{ji} are explicitly available and not merely bounded as in Lemma 10. Summing up these stage times exactly is therefore an immediate way to obtain an improved error bound. Furthermore, the triangle inequality on $\|R^{(p)}(\tau)\|$ in the proof of Lemma 12 is a crude overestimate: it loses information about (i). terms that could cancel between the two multiindex sums, and (ii.) any commutation relations between the individual trotter stages.

In the following subsection, we will provide a tighter error analysis, featuring more optimal but less clean analytical expressions which we can nonetheless evaluate efficiently numerically.

4.4 Explicit Summation of Trotter Stage Coefficients

For the recursive Suzuki-Trotter formula in Eq. (24) we can immediately improve the error bound by summing the stage coefficients b_{ij} up exactly, instead of bounding them as in Lemma 10.

Corollary 14 (Trotter Error). *For the recursive product formula in Eq. (24) and $p = 2k$ for $k \geq 1$,*

$$\epsilon_p(T, \delta) \leq \frac{2T\delta^p M^{p+1} \Lambda^{p+1}}{(p+1)!} H_p^{p+1} \quad \text{where} \quad H_p := \prod_{i=1}^{p/2-1} \frac{4 + 4^{1/(2i+1)}}{|4 - 4^{1/(2i+1)}|}.$$

Proof. This follows from explicitly summing up the magnitudes of all the b_{ji} 's obtained by solving the recursive definition of the product formula, which can easily be verified to satisfy $\sum_{ij} |b_{ij}(p)| = MH_p$. Then from Lemma 12,

$$\|R^{(p)}(\tau)\| \leq 2\Lambda^{p+1} \sum_{\alpha: |\alpha|=p+1} \binom{p+1}{\alpha} \prod_{j=1}^S \prod_{i=1}^M |b_{ji}^{\alpha_{ij}}| = 2\Lambda^{p+1} \left(\sum_{j=1}^S \sum_{i=1}^M |b_{ji}| \right)^{p+1},$$

and the claim follows as before. \square

For later reference, we note that it is straightforward to generalise the error bound in Corollary 14 for the case of a *higher* derivative $R^{(q)}$, $q \geq p$, but still for a p^{th} order formula: the bound simply reads

$$\epsilon_{p,q}(T, \delta) \leq \frac{2T\delta^q M^{q+1} \Lambda^{q+1}}{(q+1)!} H_p^{q+1}. \quad (37)$$

4.5 Commutator Bounds

Our analysis thus far has completely neglected the underlying structure of the Hamiltonian. In this subsection we establish commutator bounds which are easily applicable to D -dimensional lattice Hamiltonians.

We begin with the following technical lemmas.

Lemma 15. *For a product formula accurate to p^{th} order, having $S = S_p$ stages for M non-commuting Hamiltonian layers with the upper-bound $\|H_i\| = \Lambda_I$, the error term $R(\tau)$ satisfies*

$$\left\| \frac{\partial^p}{\partial \tau^p} R(\tau) \right\| \leq \sum_J \sum_{\beta: |\beta|=p} \binom{p}{\beta} \sum_{I=J+1}^{SM} (B_p \Lambda)^{p-\beta_I} \left\| \left[U_J^{(1)}(0), U_I^{(\beta_I)}(\tau) \right] \right\|.$$

Proof. As shown in Lemma 12,

$$R^{(p)}(\tau) = \sum_{\alpha: |\alpha|=p+1} \binom{p+1}{\alpha} \prod_I U_I^{(\alpha_I)}(\tau) - \sum_J U_J^{(1)}(0) \sum_{\beta: |\beta|=p} \binom{p}{\beta} \prod_I U_I^{(\beta_I)}(\tau).$$

We begin by commuting every $U_J^{(1)}(0)$ past $\prod_{I=J+1}^{SM} U_I^{(\beta_I)}(\tau)$. Consider this for some fixed J in the sum of over J . That is consider rewriting a particular summand from the second term above to obtain

$$\begin{aligned} & U_J^{(1)}(0) \sum_{\beta: |\beta|=p} \binom{p}{\beta} \prod_I U_I^{(\beta_I)}(\tau) \\ &= \sum_{\beta: |\beta|=p} \binom{p}{\beta} U_J^{(1)}(0) \left(U_{sm}^{(\beta_{sm})}(\tau) \dots U_{J+1}^{(\beta_{J+1})}(\tau) \right) \left(U_J^{(\beta_J)}(\tau) \dots U_1^{(\beta_1)}(\tau) \right) \\ &= \sum_{\beta: |\beta|=p} \binom{p}{\beta} \left(U_{sm}^{(\beta_{sm})}(\tau) \dots U_{J+1}^{(\beta_{J+1})}(\tau) \right) \left(U_J^{(\beta_J)}(\tau) \dots U_1^{(\beta_1)}(\tau) \right) \\ &\quad + \sum_{\beta: |\beta|=p} \binom{p}{\beta} \left[U_J^{(1)}(0), \prod_{I=J+1}^{SM} U_I^{(\beta_I)}(\tau) \right] \prod_{I=1}^J U_I^{(\beta_I)}(\tau) \end{aligned}$$

Now, by inserting this into the full expression for $R^{(p)}(\tau)$, we obtain

$$\begin{aligned} R^{(p)}(\tau) &= \sum_{\alpha: |\alpha|=p+1} \binom{p+1}{\alpha} \prod_I U_I^{(\alpha_I)}(\tau) - \sum_{\beta: |\beta|=p+1} \binom{p+1}{\beta} \prod_I U_I^{(\beta_I)}(\tau) \\ &\quad - \sum_J \sum_{\beta: |\beta|=p} \binom{p}{\beta} \left[U_J^{(1)}(0), \prod_{I=J+1}^{SM} U_I^{(\beta_I)}(\tau) \right] \prod_{I=1}^J U_I^{(\beta_I)}(\tau) \\ &= - \sum_J \sum_{\beta: |\beta|=p} \binom{p}{\beta} \left[U_J^{(1)}(0), \prod_{I=J+1}^{SM} U_I^{(\beta_I)}(\tau) \right] \prod_{I=1}^J U_I^{(\beta_I)}(\tau) \\ &= - \sum_J \sum_{\beta: |\beta|=p} \binom{p}{\beta} \sum_{I=J+1}^{SM} \prod_{K=I+1}^{SM} U_K^{(\beta_K)} \left[U_J^{(1)}(0), U_I^{(\beta_I)}(\tau) \right] \prod_{K=1}^{I-1} U_K^{(\beta_K)} \end{aligned}$$

Taking the norm of this expression gives

$$\begin{aligned} \left\| \frac{\partial^p}{\partial \tau^p} R(\tau) \right\| &\leq \sum_J \sum_{\beta: |\beta|=p} \binom{p}{\beta} \sum_{I=J+1}^{SM} (B_p \Lambda)^{\sum_{K=I+1}^{SM} \beta_K} \left\| \left[U_J^{(1)}(0), U_I^{(\beta_I)}(\tau) \right] \right\| (B_p \Lambda)^{\sum_{K=1}^{I-1} \beta_K} \\ &= \sum_J \sum_{\beta: |\beta|=p} \binom{p}{\beta} \sum_{I=J+1}^{SM} (B_p \Lambda)^{p-\beta_I} \left\| \left[U_J^{(1)}(0), U_I^{(\beta_I)}(\tau) \right] \right\| \end{aligned}$$

This completes the proof. \square

Lemma 16. *If every pair of Hamiltonians can be written as $H_I = \sum_{i=1}^N h_i^I$ and $H_J = \sum_{i=1}^N h_i^J$, where for any i we have $\|h_i^I\| = \|h_i^J\| = 1$ and for any fixed term h^J there are at most n terms in H_I which do not commute with that specific term, then*

$$\left\| \left[U_J^{(1)}(0), U_I^{(\beta_I)}(0) \right] \right\| \leq 2n\beta_I N^{\beta_I} B_p^{\beta_I+1}.$$

Proof. First note that

$$U_J^{(1)}(0) = -ib_J H_J = -ib_J \sum_{i=1}^N h_i^J$$

and

$$U_I^{(\beta_I)}(0) = (-ib_I H_I)^{\beta_I} = (-ib_I)^{\beta_I} \left(\sum_{i=1}^N h_i^I \right)^{\beta_I}.$$

Consider a fixed term in $U_J^{(1)}(0)$ such as $-ib_J h^J$, where we have dropped the subscript i . As there are N of these, we can bound the norm of the commutator as follows

$$\left\| \left[U_J^{(1)}(0), U_I^{(\beta_I)}(0) \right] \right\| \leq N B_p \left\| \left[h^J, U_I^{(\beta_I)}(0) \right] \right\|$$

using the triangle inequality and the fact that $b_J \leq B_p$.

Now consider fully expanding the $U_I^{(\beta_I)}$ so that it is a sum of N^{β_I} norm 1 Hamiltonians with coefficients upper-bounded by $(B_p)^{\beta_I}$. As only n of the N normalised Hamiltonians do not commute with h^J , the number of Hamiltonians in the expanded $U_I^{(\beta_I)}$ which do not commute with h^J can be upper-bounded by $n\beta_I N^{\beta_I-1}$. Here we have assumed that if any of the n non-commuting terms appear at any point in the expansion (the n), then that term will not commute with h^J regardless of whatever other terms appear (the N^{β_I-1}). We can over-count by repeating this for each term expanded (the β_I). This gives

$$\left\| \left[U_J^{(1)}(0), U_I^{(\beta_I)}(0) \right] \right\| \leq 2n\beta_I N^{\beta_I} B_p^{\beta_I+1}.$$

The extra factor of 2 comes from bounding the commutators of the norm 1 Hamiltonians via triangle inequality. \square

Lemma 17. *If every pair of Hamiltonians can be written as $H_I = \sum_{i=1}^N h_i^I$ and $H_J = \sum_{i=1}^N h_i^J$, where all $\|h_i^I\| = \|h_i^J\| = 1$, and if additionally for any fixed term h^J there are at most n terms h^I which do not commute with h^J , then*

$$\begin{aligned} \left\| \frac{\partial^p}{\partial \tau^p} R(\tau) \right\| &\leq np B_p^{p+1} \Lambda^{p-1} N \left((SM-1) + \frac{N}{\Lambda} \right)^{p-1} \left((SM)^2 - (SM) \right) \\ &\quad + n\tau B_p^{p+2} \Lambda^p N e^{\tau N B_p} \left((SM)^{p+2} - (SM)^{p+1} \right). \end{aligned}$$

Proof. We must obtain a simplified form for the bounded commutator appearing in Lemma 15. We can sequentially expand this commutator and use the triangle inequality to write it as

$$\begin{aligned} \left\| \left[U_J^{(1)}(0), U_I^{(\beta_I)}(\tau) \right] \right\| &= \left\| \left[U_J^{(1)}(0), U_I^{(\beta_I)}(0) e^{i\tau b_I H_I} \right] \right\| \\ &\leq \left\| \left[U_J^{(1)}(0), U_I^{(\beta_I)}(0) \right] \right\| + B_p^{\beta_I} \Lambda^{\beta_I} \left\| \left[U_J^{(1)}(0), e^{i\tau b_I H_I} \right] \right\|. \end{aligned}$$

We can use Lemma 16 to bound the first term. The commutator in the second term can be bounded as follows:

$$\begin{aligned} \left\| \left[U_J^{(1)}(0), e^{i\tau b_I H_I} \right] \right\| &= \left\| \left[U_J^{(1)}(0), \mathbb{1} + i\tau b_I H_I + \frac{1}{2!} (i\tau b_I H_I)^2 + \dots \right] \right\| \\ &\leq \sum_{k=1}^{\infty} \frac{\tau^k}{k!} \left\| \left[U_J^{(1)}(0), U_I^{(k)}(0) \right] \right\| \\ &\leq \sum_{k=1}^{\infty} \frac{2n\tau^k}{(k-1)!} N^k B_p^{k+1} \\ &= 2n\tau N B_p^2 e^{N B_p \tau}. \end{aligned}$$

Where we have used Lemma 16 to bound the norm of the commutator of $U_J^{(1)}(0)$ and $U_I^{(k)}(0)$ by $2nkN^k B_p^{k+1}$ and simplified the resulting expression. The first term can be bounded directly with Lemma 16, so we obtain

$$\left\| \left[U_J^{(1)}(0), U_I^{(\beta_I)}(\tau) \right] \right\| \leq 2n\beta_I N^{\beta_I} B_p^{\beta_I+1} + 2n\tau N \Lambda^{\beta_I} B_p^{2+\beta_I} e^{N B_p \tau}.$$

Now by using this to bound the result of Lemma 15 we obtain

$$\begin{aligned} \left\| \frac{\partial^p}{\partial \tau^p} R(\tau) \right\| &\leq \sum_J \sum_{\beta: |\beta|=p} \binom{p}{\beta} \sum_{I=J+1}^{SM} (B_p \Lambda)^{p-\beta_I} \left\| \left[U_J^{(1)}(0), U_I^{(\beta_I)}(\tau) \right] \right\| \\ &\leq \sum_J \sum_{\beta: |\beta|=p} \binom{p}{\beta} \sum_{I=J+1}^{SM} (B_p \Lambda)^{p-\beta_I} \left(2n\beta_I N^{\beta_I} B_p^{\beta_I+1} + 2n\tau N \Lambda^{\beta_I} B_p^{2+\beta_I} e^{N B_p \tau} \right) \\ &= \sum_J \sum_{\beta: |\beta|=p} \binom{p}{\beta} \sum_{I=J+1}^{SM} \left(2n\beta_I \left(\frac{N}{\Lambda} \right)^{\beta_I} \Lambda^p B_p^{p+1} + 2n\tau N \Lambda^p B_p^{p+2} e^{N B_p \tau} \right). \end{aligned}$$

To simplify this expression, we must simplify an expression of the form

$$\sum_{\beta: |\beta|=p} \binom{p}{\beta} \beta_I x^{\beta_I}$$

where in our case $x = N/\Lambda$. This can be done by rewriting this expression in terms of a derivative with respect to x and reversing the multinomial theorem, which gives

$$\begin{aligned} \sum_{\beta: |\beta|=p} \binom{p}{\beta} \beta_I x^{\beta_I} &= x \frac{d}{dx} \sum_{\beta: |\beta|=p} \binom{p}{\beta} x^{\beta_I} \\ &= x \frac{d}{dx} \left(\underbrace{1 + \dots + 1 + x}_{SM \text{ terms}} \right)^p \\ &= px (SM - 1 + x)^{p-1}. \end{aligned}$$

Using this and performing the summation over J and I simplifies the expression for $\|R^{(p)}(\tau)\|$ to

$$\begin{aligned} \left\| \frac{\partial^p}{\partial \tau^p} R(\tau) \right\| &\leq pn B_p^{p+1} \Lambda^{p-1} N \left(SM - 1 + \frac{N}{\Lambda} \right)^{p-1} \left((SM)^2 - (SM) \right) \\ &\quad + \tau n B_p^{p+2} \Lambda^p N \left((SM)^{p+2} - (SM)^{p+1} \right) e^{\tau N B_p}. \end{aligned}$$

□

Now we can use the preceding lemmas to establish a commutator bound for higher order Trotter formulae. Although it is cumbersome looking, it is easy to evaluate.

Theorem 18 (Commutator Error Bound). *Let $H = \sum_{i=1}^M H_i$ with $\|H_i\| \leq \Lambda$ be a Hamiltonian with M mutually commuting layers $H_I = \sum_{i=1}^N h_i^I$. Assume that for any i , $\|h_i^I\| = \|h_i^J\| \leq 1$. Additionally, assume that for any fixed term h^J there exist at most n terms h^I which do not commute with h^J .*

Then, for a p^{th} order product formula \mathcal{P}_p with $p = 1$ or $p = 2k$, $k \geq 1$ used to approximate the evolution operator under H , the approximation error for the exact evolution $U(T)$ with T/δ rounds of the product formula $\mathcal{P}_p(\delta)$ is bounded by

$$\epsilon_p(T, \delta) \leq C_1 \frac{T \delta^p}{(p+1)!} + C_2 \frac{T}{\delta} \int_0^\delta p \int_0^1 (1-x)^{p-1} \frac{x \tau^{p+1}}{p!} e^{x \tau N B_p} dx d\tau$$

with

$$\begin{aligned} C_1 &= np B_p^{p+1} \Lambda^{p-1} N \left((SM - 1) + \frac{N}{\Lambda} \right)^{p-1} \left((SM)^2 - (SM) \right) \\ C_2 &= n B_p^{p+2} \Lambda^p N \left((SM)^{p+2} - (SM)^{p+1} \right). \end{aligned}$$

Proof. The error formula for a single Trotter step is given by Eq. (33) as

$$\epsilon_p(\delta) \leq p \int_0^\delta \int_0^1 (1-x)^{p-1} \|R^{(p)}(x\tau)\| \frac{\tau^p}{p!} dx d\tau.$$

Evaluating this using Lemma 17 and then substituting the resultant expression in $\epsilon_p(T, \delta) \leq (T/\delta)\epsilon_p(\delta)$ gives the stated expression. \square

For later reference, we note that it is straightforward to generalise the error bound in Theorem 18, by incorporating similar techniques to Corollary 14 in order to sum up the $|b_{ij}|$ exactly, instead of simply bounding them by B_p . Additionally, we can also generalise to the case of a *higher* derivative $R^{(q)}$, $q \geq p$, but still for a p^{th} order formula: with these two generalisations the bound simply reads

$$\epsilon_{p,q}(T, \delta) \leq C_1 \frac{T\delta^q}{(q+1)!} + C_2 \frac{T}{\delta} \int_0^\delta q \int_0^1 (1-x)^{q-1} \frac{x\tau^{q+1}}{q!} e^{x\tau NB_p} dx d\tau$$

with

$$\begin{aligned} C_1 &= nqB_p^2\Lambda^{q-1}N \left(MH_p - B_p + B_p \left(\frac{N}{\Lambda} \right) \right)^{q-1} \left((S_p M)^2 - (S_p M) \right) \\ C_2 &= nB_p^2 (MH_p\Lambda)^q N \left((S_p M)^2 - (S_p M) \right). \end{aligned}$$

4.6 A Taylor Bound on the Taylor Bound

Another method to obtain a tighter bound on a Taylor expansion as used on $R(\tau)$ in Eq. (30) and which can be used together with the more sophisticated commutator-based error bound from Theorem 18 derived in the last section, can be obtained by performing a Taylor expansion of the remainder term, and in turn bounding *its* Taylor remainder by some other method [Bau12, Rem. 4].

We first establish the following technical lemma:

Lemma 19 (Taylor Error Bound). *Let the setup be as in Lemma 12, and let $q > p$. The error term ϵ from Eq. (27) satisfies*

$$\epsilon_p(\delta) \leq \sum_{l=p}^q \frac{\delta^{l+1}}{(l+1)!} \|R^{(l)}(0)\| + \epsilon_{p,q+1}(\delta)$$

where

$$R(0)^{(l)} = \sum_{\alpha: |\alpha|=p+1} \binom{p+1}{\alpha} F(\alpha) + iH \sum_{\beta: |\beta|=p} \binom{p}{\beta} F(\beta),$$

with $H = \sum_{i=1}^M H_i$, and

$$F(\alpha) := \prod_{j=1}^S \prod_{i=1}^M (-ib_{ji}H_i)^{\alpha_{(i,j)}}.$$

Proof. The expression for ϵ stems from Taylor-expanding Eq. (33) to order q instead of p , and integrating over τ . The last term $\epsilon_{q+1,p}$ is then simply the overall remainder S , as before; and we can use Eq. (37) to obtain a bound on it. The bound on $\|R(0)^{(l)}\|$ is an immediate consequence of Eq. (36), where we set $\tau = 0$. \square

This allows us to calculate a numerical bound on $\|R(0)^{(l)}\|$, by bounding $\|H_i\| \leq \Lambda$ and allowing terms within the two sums over α and β to cancel. The benefit of this approach is that it is generically applicable to any given Trotter formula, and only depends on the non-commuting layers of H .

We can therefore derive the following bounds:

Corollary 20 (Taylor Error Bound). *Let $H = \sum_{i=1}^M H_i$ with $\|H_i\| \leq \Lambda$ for all i . Then for ϵ from Eq. (33), and for a p^{th} Trotter formula, we have*

$$\epsilon_p(\delta) \leq \sum_{l=p}^q \frac{\delta^{l+1} \Lambda^{l+1}}{(l+1)!} f(p, M, l) + \epsilon_{p,q+1}(\delta),$$

where

$$f(p, M, l) = \left\| \sum_{\alpha: |\alpha|=p+1} \binom{p+1}{\alpha} v(\alpha) + i \sum_{j=1}^M |j\rangle \otimes \sum_{\beta: |\beta|=p} \binom{p}{\beta} v(\beta) \right\|_1,$$

and

$$v(\alpha) := \bigotimes_{j=1}^S \bigotimes_{i=1}^M (-ib_{ji} |i\rangle)^{\otimes \alpha_{(i,j)}}.$$

for a basis $\{|1\rangle, \dots, |M\rangle\}$ of \mathbb{C}^M .

Proof. Follows immediately from Lemma 19. \square

A selection of the series coefficients $f(p, M, l)$ can be found in Table 2. Corollary 20 can then be applied in conjunction with e.g. the commutator error bound given in Theorem 18 for the remaining term $\epsilon_{q+1}(\delta, \delta)$.

		$f(p, M, l)$ for $l = \cdot$					
	M	$l=p$	$l=p+1$	$l=p+2$	$l=p+3$	$l=p+4$	$l=p+5$
p=1	2	2	6	14	30	62	126
	3	6	26	90	290	906	2786
	4	12	68	312	1340	5592	22988
	5	20	140	800	4292	22400	115220
p=2	2	3	9	22.75	50	108.344	225.531
	3	13	57	213.25	711.25	2309.47	7283.06
	4	34	198	980.5	4377.5	18926.6	79758
	5	70	510	3141.5	17555	94765.3	499391
p=4	2	4.89745	19.5277	79.5305	442.266	2312.73	11208.3
	3	43.6604	277.994	1880.62	16924.7		
	4	194.476	1719.69	16226.8			
	5	610.187	6926.95	83775.9			

Table 2: Trotter error coefficients $f(p, M, l)$ from Corollary 20; values rounded to the precision shown.

5 Spectral Norm of Fermionic Hopping Terms

Let a^\dagger and a be the standard fermionic creation and annihilation operators.

Theorem 21. *Let $\Omega = \{ij\}$ be a set of pairs of indices such that no two pairs share an index. Define:*

$$H_\Omega = \sum_{ij \in \Omega} h_{ij}, \quad h_{ij} = a_i^\dagger a_j + a_j^\dagger a_i$$

. *Given a normalized fermionic state $|\psi\rangle$ such that $N|\psi\rangle = n|\psi\rangle$:*

$$|\langle \psi | H_\Omega | \psi \rangle| \leq \min(n, M - n, |\Omega|)$$

Where M is the number of fermionic modes. This bound is tight.

Proof. Consider that h_{ij} has eigenvalues in $\{-1, 0, 1\}$, since $h_{ij}^2 = (N_i - N_j)^2$ which has eigenvalues $\{0, 1\}$. Suppose there existed a normalized state $|\psi\rangle$ such that $N|\psi\rangle = n|\psi\rangle$ and $H_\Omega|\psi\rangle = \lambda|\psi\rangle$ where $|\lambda| > \min(n, M - n, |\Omega|)$. Since H_Y, N and all h_{ij} are all mutually commuting, we may choose $|\psi\rangle$ to be an eigenstate of all h_{ij} wlog (by convexity). Then it must be the case that $h_{ij}^2|\psi\rangle = |\psi\rangle$ for at least $|\lambda|$ pairs ij , which implies that in the fock basis $|\psi\rangle = a|0_i, 1_j, \dots\rangle + b|1_i, 0_j, \dots\rangle$. Therefore for at least $|\lambda|$ pairs $ij \in \Omega$ we have $\langle \psi | (N_i + N_j) | \psi \rangle = 1$. So $\langle \psi | N | \psi \rangle \geq |\lambda|$ and $M - \langle \psi | N | \psi \rangle \geq |\lambda|$. If $\min(n, M - n, |\Omega|) = n$ then $\langle \psi | N | \psi \rangle > n$ which is a contradiction.

If $\min(n, M - n, |\Omega|) = M - n$ then $M - \langle \psi | N | \psi \rangle > M - n$ which is a contradiction. If $\min(n, M - n, |\Omega|) = |\Omega|$ then $|\lambda| > |\Omega|$ which is a contradiction. This proves the bound.

Now we need only show the bound is tight. Consider the following state:

$$\left| \phi_{ij}^\pm \right\rangle = (a_i^\dagger \pm a_j^\dagger) \Gamma_s |0\rangle$$

With Γ_s composed of creation and annihilation operators which do not include i or j . This state is an eigenstate of $h_{ij} = a_i^\dagger a_j + a_j^\dagger a_i$:

$$h_{ij} \left| \phi_{ij}^\pm \right\rangle = \pm \left| \phi_{ij}^\pm \right\rangle$$

proof:

$$\begin{aligned} h_{ij} \left| \phi_{ij}^\pm \right\rangle &= h_{ij} (a_i^\dagger \pm a_j^\dagger) \Gamma_s |0\rangle \\ &= (a_i^\dagger a_j a_i^\dagger + a_j^\dagger a_i a_i^\dagger \pm a_i^\dagger a_j a_j^\dagger \pm a_j^\dagger a_i a_j^\dagger) \Gamma_s |0\rangle \\ &= (a_j^\dagger a_i a_i^\dagger \pm a_i^\dagger a_j a_j^\dagger) \Gamma_s |0\rangle \\ &= ((-a_j^\dagger a_i^\dagger a_i + a_j^\dagger) \pm (-a_i^\dagger a_j^\dagger a_j + a_i^\dagger)) \Gamma_s |0\rangle \\ &= (a_j^\dagger \pm a_i^\dagger) \Gamma_s |0\rangle \\ h_{ij} \left| \phi_{ij}^\pm \right\rangle &= \pm (a_i^\dagger \pm a_j^\dagger) \Gamma_s |0\rangle \end{aligned}$$

Consider a set of pairs of indices $\omega \subseteq \Omega$. Choose an ordering on ω and define

$$\left| \phi_\omega^b \right\rangle = \prod_{ij \in \omega} (a_i^\dagger + (-1)^{b_{ij}} a_j^\dagger) |0\rangle$$

with b a bitstring indexed by ij . Note that $N \left| \phi_\omega^b \right\rangle = |\omega| \left| \phi_\omega^b \right\rangle$. We now argue that b can always be chosen such that:

$$H_\Omega \left| \phi_\omega^b \right\rangle = |\omega| \left| \phi_\omega^b \right\rangle.$$

Choose a pair $ij \in \omega$, the state $\left| \phi_\omega^b \right\rangle$ can be expressed as:

$$\left| \phi_\omega^b \right\rangle = (\delta_i a_i^\dagger + (-1)^{b_{ij}} \delta_j a_j^\dagger) \Gamma_s |0\rangle, \quad \delta_i, \delta_j \in \{-1, 1\}$$

With Γ_s composed of creation and annihilation operators which do not include i or j . So

$$\left| \phi_\omega^b \right\rangle = \delta_i \left| \phi_{ij}^{\Delta_{ij}} \right\rangle, \quad \Delta_{ij} = \delta_i \delta_j (-1)^{b_{ij}}.$$

Let us choose b_{ij} such that $\Delta_{ij} = 1$. Noting that Δ_{ij} is independent of Δ_{pq} when $pq \neq ij$ we can do the same for all other b_{pq} . This gives:

$$H_\Omega \left| \phi_\omega^b \right\rangle = \sum_{ij \in \omega} h_{ij} \delta_i \left| \phi_{ij}^+ \right\rangle$$

$$H_{\Omega} |\phi_{\omega}^b\rangle = \sum_{ij \in \omega} \delta_i |\phi_{ij}^+\rangle$$

$$H_{\Omega} |\phi_{\omega}^b\rangle = \sum_{ij \in \omega} |\phi_{\omega}^b\rangle$$

$$H_{\Omega} |\phi_{\omega}^b\rangle = |\omega| |\phi_{\omega}^b\rangle$$

Note that $n = |\omega| < |\Omega|$ and $|\Omega| < M/2$ and so the bound is shown to be tight in the case where $\min(n, M - n, |Y|) = n$.

If we consider the case where $\min(n, M - n, |\Omega|) = |\Omega|$, then we may always choose ω such that it is composed of a set of pairs of indices such that no two pairs share an index, and such that $\Omega \subseteq \omega$. In this case, by a similar argument

$$H_{\Omega} |\phi_{\omega}^b\rangle = |\Omega| |\phi_{\omega}^b\rangle.$$

Finally, in the case where $\min(n, M - n, |\Omega|) = M - n$ one may choose the particle-hole symmetric state

$$|\tilde{\phi}_{\omega}^b\rangle = \prod_{ij \in \omega} (a_i + (-1)^{b_{ij}} a_j) \prod_{k=1}^M a_k^{\dagger} |0\rangle$$

and a similar argument follows by particle hole symmetry. \square

6 Simulating Fermi-Hubbard via Sub-Circuit Algorithms

6.1 Overview and Benchmarking of Analysis

In this section we establish asymptotic bounds on the run-time $\mathcal{T}_{\text{cost}}$, according to Definition 2, of performing a time-dynamics simulation of a 2D spin Fermi-Hubbard Hamiltonian using a p^{th} -order Trotter formula with $M = 5$ Trotter layers, for a target time T and target error ϵ_r . We perform this analysis for both the LW and VC encodings and the results are summarised in Remark 24.

We want to benchmark our proposals—sub-circuit Trotter step synthesis and constants optimised Trotter bounds—as fairly as possible. So to this end we establish the analytic bounds for the same simulation task, but using the standard conjugation method to generate evolution under higher weight interactions, and not our sub-circuit pulse sequence identities. We choose this method as it doesn't introduce any unfair and needless analytic error into the comparison and as it is equivalent to decomposing the Trotter steps into a standard gate set of CNOTs and single-qubit rotations as we completely decompose every trotter step into gates of the form $e^{\pm i\pi/4ZZ}$. We cost this with the same metric, but do not allow the comparison to contain any gates of the form $e^{\pm i\delta ZZ}$.

In this comparative analytic expression we still use our Trotter error bounds, so Remark 23 only serves to evaluate the impact of differing Trotter step synthesis methods on the asymptotic scaling of the run-time $\mathcal{T}_{\text{cost}}$.

Later in this section we perform a tighter numerical analysis of both our proposal and our standard circuit model comparison. In these numerics we compare our Trotter bounds to readily applicable bounds from the literature [Chi+17, Prop. F.4.]. We point out that these bounds do not exploit the underlying structure of the Hamiltonian or make use of the recent advances of [CS19], [Chi+19]. However these bounds contained the full expressions up to all constants, were applicable to 2D lattices and could easily be evaluated for arbitrary p and allowed us to make use of Section 5. We were able to compare our bounds to [CS19] for the case of a simple 1D lattice and establish that our bounds are preferable for medium system sizes, not in asymptotic limits of system size, as was our intention in reformulating bounds for NISQ applications.

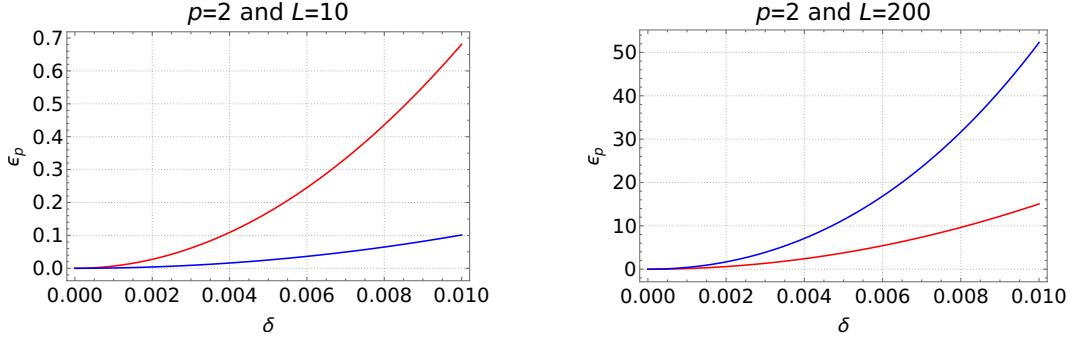


Figure 8: A comparison of 2nd order Trotter bounds $\epsilon_p(\delta, L)$ for a 1D lattice Hamiltonian of length L split into even and odd layers of interactions $H = H_{\text{even}} + H_{\text{odd}}$. The bounds are our Theorem 18 (blue) and the main result stated in [CS19] which we’ve evaluated from [CS19, Sec. B:eq. 57+58] (red). This illustrates why we have derived Trotter bounds which sacrifice scaling in system size in favour of bounds with smaller constants in term of p . Here we evaluate Theorem 18 with $\Lambda = L/2$ as this illustrative example is a generic, not fermionic, lattice Hamiltonian.

6.2 The Fermi-Hubbard Hamiltonian and Fermionic Encodings

We consider a Fermi-Hubbard model on a 2D lattice of $N = L \times L$ fermionic sites. There is hopping between nearest neighbours only and on-site interactions between fermions of opposite spin. In terms of fermionic creation and annihilation operators the Hamiltonian for this system is

$$H_{\text{FH}} := \sum_{i=1}^N h_{\text{on-site}}^{(i)} + \sum_{i < j, \sigma} h_{\text{hopping}}^{(i,j,\sigma)} := u \sum_{i=1}^N a_{i\uparrow}^\dagger a_{i\uparrow} a_{i\downarrow}^\dagger a_{i\downarrow} + v \sum_{i < j, \sigma} \left(a_{i\sigma}^\dagger a_{j\sigma} + a_{j\sigma}^\dagger a_{i\sigma} \right), \quad (38)$$

where $\sigma \in \{\uparrow, \downarrow\}$ and the sum over hopping terms runs over all nearest neighbour fermionic lattice sites i and j . The interaction strengths are u and v and we assume that $v = 1$, and that they are bounded as $|v|, |u| \leq r$. Before we proceed we have to choose how to encode this Hamiltonian in

terms of spin operators. The choice of encoding has a significant impact on the run-time of the simulation. There are many encodings in the literature [JW28] but we will only analyse two, the Verstraete-Circa (VC) encoding [VC05], and the recent low-weight (LW) encoding from [DK20].

We choose our encoding in order to minimise the maximum Pauli weight of the encoded interaction terms. Using the VC and LW encodings this is constant at weight-4 and weight-3 respectively. In comparison the Jordan-Wigner encoding results in a maximum Pauli weight of the encoded interaction terms that scales with the lattice size as $O(L)$, the Bravyi-Kitaev encoding [BK02] has interaction terms of weight $O(\log L)$, and the Bravyi-Kitaev superfast encoding [BK02] results in weight-8.

The encodings require the addition of ancillary qubits as well as two separate lattices encoding spin up and spin down fermions. For VC $4L^2$ qubits are needed to encode L^2 fermionic sites. In contrast LW requires $(L-1)^2$ ancillary qubits and $2L^2$ data qubits. The layout of these ancillary qubits are indicated in Fig. 9. Note that we must also choose an ordering of the lattice sites. This is also indicated in Fig. 9.

The two encodings map the Fermi-Hubbard Hamiltonian terms to interactions between qubits. In both encodings, on-site interaction terms become

$$h_{\text{on-site}}^{(i)} \rightarrow \frac{u}{4} (\mathbb{1} - Z_{i\uparrow}) (\mathbb{1} - Z_{i\downarrow}). \quad (39)$$

Only the encoded hopping terms differ. The exact expressions for hopping interactions depend on whether two nearest neighbour fermionic sites are horizontally or vertically connected on the lattice. The horizontally connected hopping terms are encoded as

$$h_{\text{hopping,hor}}^{(i,j,\sigma)} \rightarrow \frac{1}{2} \begin{cases} X_{i,\sigma} Z_{i',\sigma} X_{j,\sigma} + Y_{i,\sigma} Z_{i',\sigma} Y_{j,\sigma} & \text{VC} \\ X_{i,\sigma} X_{j,\sigma} Y_{f'_{ij},\sigma} + Y_{i,\sigma} Y_{j,\sigma} Y_{f'_{ij},\sigma} & \text{LW} \end{cases} \quad (40)$$

while the vertically connected hopping terms are encoded as

$$h_{\text{hopping,vert}}^{(i,j,\sigma)} \rightarrow \frac{1}{2} \begin{cases} X_{i,\sigma} Y_{i',\sigma} Y_{j,\sigma} X_{j',\sigma} - Y_{i,\sigma} Y_{i',\sigma} X_{j,\sigma} X_{j',\sigma} & \text{VC} \\ (-1)^{g(i,j)} (X_{i,\sigma} X_{j,\sigma} X_{f'_{ij},\sigma} + Y_{i,\sigma} Y_{j,\sigma} X_{f'_{ij},\sigma}) & \text{LW} \end{cases} \quad (41)$$

In this notation i labels the data qubit for lattice site i and σ its spin lattice. Dashed indices such as i' refer to ancillary qubits. These are illustrated in grey in Fig. 9. In the VC encoding there is an ancillary qubit for every site on each spin lattice. In LW these ancillary qubits are laid out in a checker-board pattern on the faces on each spin lattice. Here f'_{ij} labels the ancillary qubit to i and j . There is also a sign determined by $g(i, j) = 0, 1$. The details of this can be found in [DK20].

6.3 Choice of Trotter Layers

We group the interactions into 5 Trotter layers. Every pair of interactions within a layer must be disjoint. Under the assumptions of Definition 1 all interactions within a single layer can then be

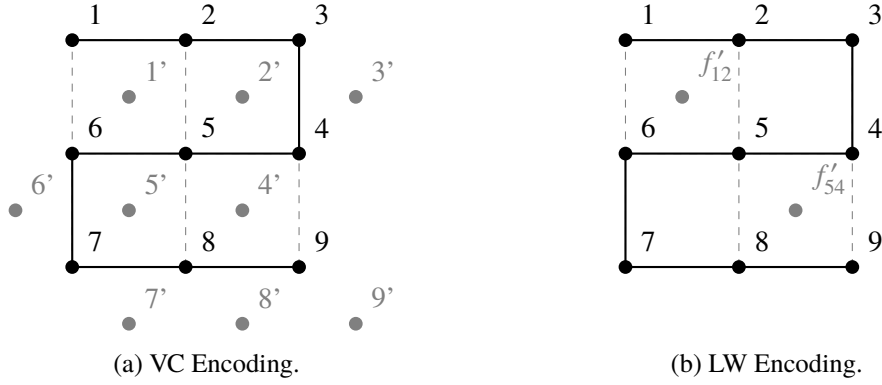


Figure 9: The ordering of qubits for $L = 2$ and the layout of ancillary qubits (grey) for each encoding. This figure only depicts a single spin lattice. Additionally, the first VC ancillary qubit f'_{12} is also labelled by f'_{25} , f'_{56} and f'_{16} . Similarly for the other (VC) ancillary qubit.

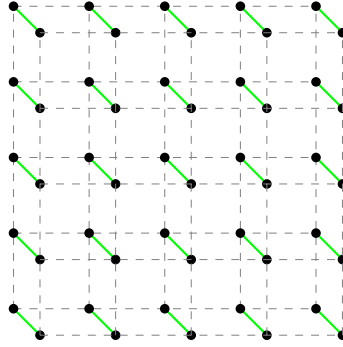


Figure 10: The green lines connecting pairs of qubits represent a single on-site interaction term in either encoding $h^{(i)}_{\text{on-site}}$.

implemented in parallel. For both encodings the five layers consist of all on-site interactions H_5 , two alternating layers of horizontal hopping interactions H_1 and H_2 and, two alternating layers of vertical hopping interactions H_3 and H_4 . Both cases are illustrated in Figs. 11 to 14 for the case of $L = 5$.

The on-site interaction terms are the same in both cases and do not involve any ancillary qubits. They are shown in Fig. 10, where the ancillary qubits are consequently not depicted. The hopping terms all act within a single spin lattice. They are shown for the VC encoding in Fig. 11 and Fig. 12 for a single spin lattice, and for LW these are shown in Fig. 13 and Fig. 14

The alternating horizontal layers and alternating vertical layers are chosen to ensure that all pairs of interactions are disjoint and not just commuting. Note that we could have chosen to lay

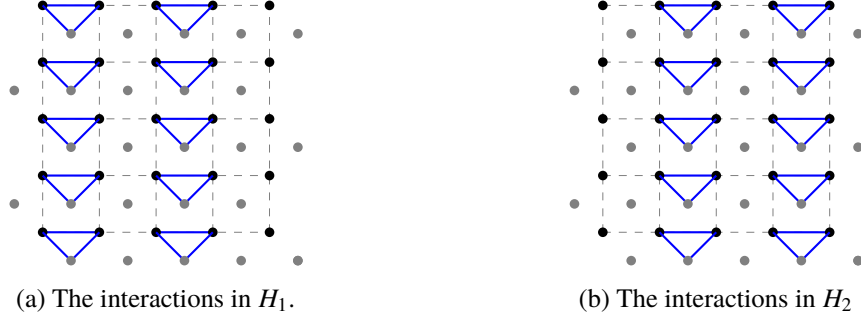


Figure 11: The blue lines connecting three qubits represent a single horizontal hopping term in the VC encoding: $h_{\text{hopping,hor}}^{(i,j,\sigma)}$

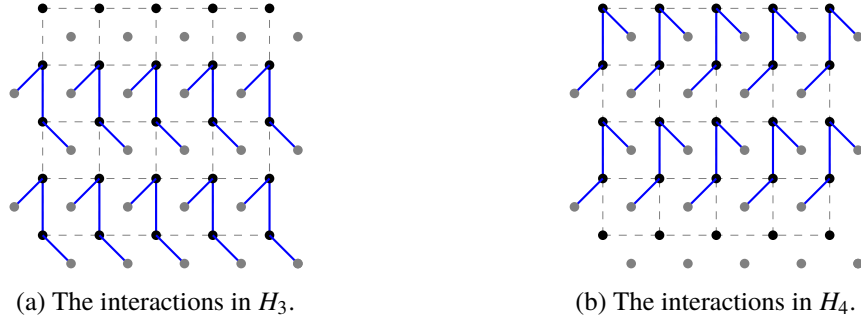


Figure 12: The blue lines connecting four qubits represent a single vertical hopping term in the VC encoding: $h_{\text{hopping,vert}}^{(i,j,\sigma)}$

out the alternating horizontal and vertical layers in the VC encoding in the same fashion as the LW as depicted in Fig. 13 or Fig. 14.

These are not the only choices of Trotter layers. In Section 7 we show that we can implement a p^{th} order product formula with only 3 Trotter layers. We do this for the LW encoding only as it is particularly neat. This is despite grouping the interactions in a way where not all interactions within a layer commute with one another. A combination of the results in Section 3 still enable us to directly implement each layer without incurring any further analytic error.

The norm of these layers appears in the Trotter bounds of Section 4. We bound these as $\|H_i\| \leq \Lambda$ for all i . In Section 5 it is shown that Λ can be related to fermion number and this fact is used to obtain tighter bounds on the Trotter error in the numerics we perform. We confine ourselves to a sector of 5 fermions in all our numerical calculations. We do this both for pragmatic reasons, since the Hilbert space dimension is just large enough to be classically hard, and because for a 5×5 lattice a roughly quarter-filling already implies interesting crossover phenomena appear [KMS01; KO14]. We also leave Λ explicit in our analytic bounds so that we can explore different parameter regions in later work.



Figure 13: The red lines connecting three qubits represent a single horizontal hopping term in the LW encoding $h_{\text{hopping,hor}}^{(i,j,\sigma)}$.



Figure 14: The red lines connecting three qubits represent a single vertical hopping term in the LW encoding: $h_{\text{hopping,vert}}^{(i,j,\sigma)}$.

6.4 Analytic Run-Time Bounds for Simulating Fermi Hubbard

Now we can proceed with obtaining analytic bounds on the run-time of this simulation for each encoding. For the recursive product formula in Eq. (24) with either $p = 1$ or $p = 2k$ for $k \geq 1$ and M non-commuting Hamiltonian layers $H = \sum_{i=1}^M H_i$, the cost of the simulation in terms of the single most expensive Trotter layer is

$$\mathcal{T}_{\text{cost}} \left(\mathcal{P}_p(\delta)^{T/\delta} \right) \leq \frac{MT}{\delta} \times \mathcal{T}_{\text{cost}} \left(U_{\max}(H, \delta B_p) \right) \times \begin{cases} 1 & p = 1 \\ 2 \times 5^{p/2-1} & p = 2k \text{ for } k \geq 1, \end{cases} \quad (42)$$

where $U_{\max}(H, \tau) := \arg\max_{U_i} \{\mathcal{T}_{\text{cost}}(U_i)\}$ for $U_i := \exp(i\tau H_i)$ and B_p given in Lemma 10. This follows from the definitions of the product formula in Eq. (24).

We proceed by obtaining bounds on the run-time of the most costly Trotter layer in each encoding. This expression depends on whether we use the methods of Section 3 (summarised in Eqs. (14) and (15)) or the conjugation method (see Eq. (12)) to implement each Trotter step.

For the VC encoding the most costly layers will be the the vertical hopping layers H_3 and H_4 . As they are both a sum of disjoint terms which we assume can be performed in parallel this is

$\mathcal{T}_{\text{cost}}(U_{\text{max}}(H, \delta B_p))$		
Encoding	standard	sub-circuit
LW	2π	$4\sqrt{B_p r \delta}$
VC	3π	$12\sqrt[3]{B_p r \delta}$

Figure 15: Cost of implementing the highest weight interaction term in the encoded Fermi-Hubbard Hamiltonian. Decomposing a k -local evolution in terms of the standard CNOT conjugation method has overhead $2(k-1) \times \pi/4$. The overhead associated with sub-circuit synthesis follows from Eq. (21).

simply given by the cost of implementing a single vertical hopping interaction. Remembering that the interaction strengths satisfy $|v|, |u| \leq r$, we bound this as

$$\begin{aligned}
\mathcal{T}_{\text{cost}}(U_{\text{max}}(H_{\text{VC}}, \delta B_p)) &\leq \mathcal{T}_{\text{cost}}\left(e^{iB_p \delta \frac{r}{2}(XYXX - YYXX)}\right) \\
&= 2 \mathcal{T}_{\text{cost}}\left(e^{iB_p \delta \frac{r}{2} Z^{\otimes 4}}\right) \\
&\leq 2 \times \begin{cases} 7(\frac{r}{2} B_p \delta)^{1/3} & \text{sub-circuit} \\ 6(\frac{\pi}{4}) & \text{standard} \end{cases}
\end{aligned}$$

The second simplification follows from both terms in the interaction commuting, thus allowing them to be performed sequentially. The same is true for the LW encoding and so we have

$$\begin{aligned}
\mathcal{T}_{\text{cost}}(U_{\text{max}}(H_{\text{LW}}, \delta B_p)) &\leq \mathcal{T}_{\text{cost}}\left(e^{iB_p \delta \frac{r}{2}(XXY + YYY)}\right) \\
&= 2 \mathcal{T}_{\text{cost}}\left(e^{iB_p \delta \frac{r}{2} Z^{\otimes 3}}\right) \\
&\leq 2 \times \begin{cases} 2(2\frac{r}{2} B_p \delta)^{1/2} & \text{sub-circuit} \\ 4(\frac{\pi}{4}) & \text{standard} \end{cases}
\end{aligned}$$

The final expressions now depend only on how we decompose local Trotter steps, either in terms of CNOT gates and single qubit rotations or using circuits such as those in Fig. 5. The concrete bounds on $\mathcal{T}_{\text{cost}}(U_{\text{max}}(H, \delta B_p))$ are summarised and simplified in Fig. 15.

Substituting the bounds in Fig. 15 into Eq. (42) results in run-times $\propto O(\delta^{-1})$ and $\propto O(\delta^{\frac{2-k}{k-1}})$, assuming decomposition via Eq. (12) or Eqs. (14) and (15), respectively. As both of these expressions diverge as $\delta \rightarrow 0$ it is optimal to maximise δ with respect to an allowable analytic Trotter error ϵ_t . This is captured in the following lemma which uses the simplest bounds on Trotter error established in Section 4.

Lemma 22 (Optimal FH δ). *For a target error rate ϵ_t , the maximum Trotter step for a p^{th} formula saturating the error bound in Theorem 13 is*

$$\delta_0 = \left(\frac{\epsilon_t}{T M^{p+1} \Lambda^{p+1}} \right)^{1/p} \times \begin{cases} 1 & p = 1 \\ \left(\frac{(p+1)!}{2} \right)^{1/p} \left(\frac{3}{10} \right)^{p/2-1/2-1/p} & p = 2k \text{ for } k \geq 1. \end{cases}$$

Proof. Follows from Theorem 13 by solving for δ . \square

Now we can obtain the final analytic bounds on the total time cost of simulating the Fermi-Hubbard Hamiltonian for each of these four cases.

Remark 23 (Standard-circuit Minimised Time Cost). *If standard synthesis techniques are used to implement local Trotter steps in terms of CNOT gates and single-qubit rotations with an optimal Trotter step size δ_0 saturating Lemma 22, the simulation cost for the Fermi-Hubbard Hamiltonian with a p^{th} order Trotter formula with maximum error ϵ_t is as follows*

$$\mathcal{T}_{\text{cost}}(\mathcal{P}_p(\delta_0)^{T/\delta_0}) \leq \begin{cases} f_p M^{2+\frac{1}{p}} \Lambda^{1+\frac{1}{p}} T^{1+\frac{1}{p}} \epsilon_t^{-1/p} & \text{VC} \\ g_p M^{2+\frac{1}{p}} \Lambda^{1+\frac{1}{p}} T^{1+\frac{1}{p}} \epsilon_t^{-1/p} & \text{LW} \end{cases}$$

with

$$f_p = 3\pi \times \begin{cases} 1 & p = 1 \\ 2^{\frac{p+1}{2}} 3^{-\frac{p}{2}+\frac{1}{p}+\frac{1}{2}} 5^{p-\frac{1}{p}-\frac{3}{2}} (p+1)!^{-\frac{1}{p}} & p = 2k \text{ for } k \geq 1 \end{cases}$$

and

$$g_p = 2\pi \times \begin{cases} 1 & p = 1 \\ 2^{\frac{p+1}{2}} 3^{-\frac{p}{2}+\frac{1}{p}+\frac{1}{2}} 5^{p-\frac{1}{p}-\frac{3}{2}} (p+1)!^{-\frac{1}{p}} & p = 2k \text{ for } k \geq 1. \end{cases}$$

Proof. The proof follows by choosing δ such that the bound obtained in Lemma 22 is saturated and substituting this and the respective expressions in Fig. 15 into Eq. (42). \square

Remark 24 (Sub-Circuit Minimised Time Cost). *If sub-circuit synthesis techniques are used to implement local Trotter steps with an optimal Trotter step size δ_0 saturating Lemma 22, the simulation cost for the Fermi-Hubbard Hamiltonian with a p^{th} order Trotter formula with maximum error ϵ_t is as follows*

$$\mathcal{T}_{\text{cost}}(\mathcal{P}_p(\delta_0)^{T/\delta_0}) \leq \begin{cases} f_p r^{1/3} M^{5/3+2/(3p)} \Lambda^{2/3+2/(3p)} T^{1+2/(3p)} \epsilon_t^{-2/(3p)} & \text{VC} \\ g_p r^{1/2} M^{3/2+1/(2p)} \Lambda^{1/2+1/(2p)} T^{1+1/(2p)} \epsilon_t^{-1/(2p)} & \text{LW} \end{cases}$$

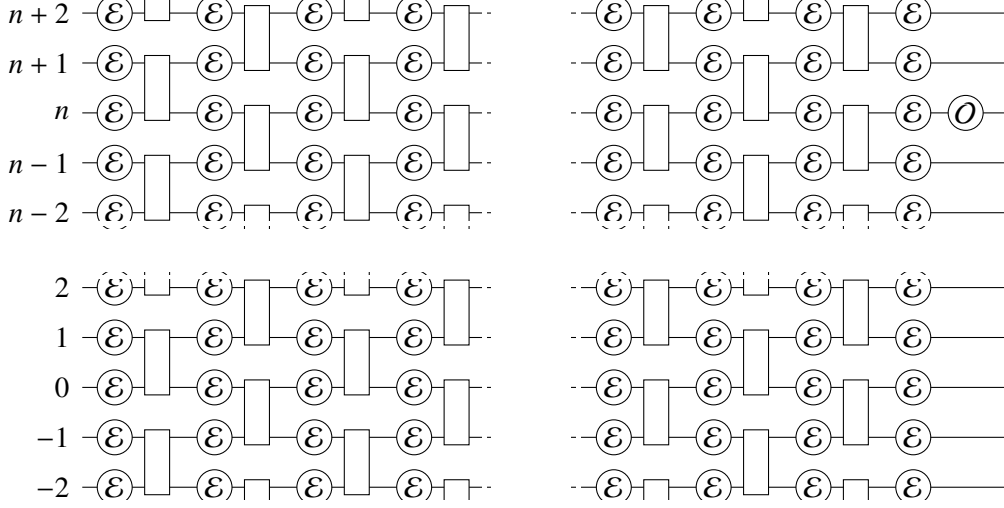


Figure 16: Saturated circuit model with intermediate errors \mathcal{E} , e.g. depolarizing noise $\mathcal{E} = \mathcal{N}_q$ for some noise parameter p given in Eq. (43). At the end of the circuit, an observable \mathcal{O} is measured. Drawn is a one-dimensional circuit; naturally, a similar setup can be derived for a circuit on a 2-dimensional qudit lattice, for interactions shown in Figs. 10 to 14.

with

$$f_p = 12 \times \begin{cases} 1 & p = 1 \\ 2^{\frac{p}{2}} 3^{\frac{1}{6}(-3p + \frac{4}{p} + 4)} 5^{\frac{1}{6}(5p - \frac{4}{p} - 8)} (p+1)!^{-\frac{2}{3p}} & p = 2k \text{ for } k \geq 1 \end{cases}$$

and

$$g_p = 4 \times \begin{cases} 1 & p = 1 \\ 2^{\frac{p}{2} - \frac{1}{4}} 3^{\frac{1}{4}(-2p + \frac{2}{p} + 3)} 5^{\frac{1}{4}(3p - \frac{2}{p} - 5)} (p+1)!^{-\frac{1}{2p}} & p = 2k \text{ for } k \geq 1. \end{cases}$$

Proof. The proof follows by choosing δ such that the bound obtained in Lemma 22 is saturated and substituting this and the respective expressions in Fig. 15 into Eq. (42). \square

6.5 Trivial Stochastic Error Bound

So far we have only considered the unitary error introduced by approximating the real Hamiltonian evolution with a Trotterized approximation. However, in a near-term quantum device without error correction in place, we expect the simulated evolution to be noisy. We model the noise by

interspersing each circuit gate in the product formula by an iid channel \mathcal{E} ; for simplicity we will assume that \mathcal{E} is a single qubit depolarizing channel $\mathcal{E} = \mathcal{N}_q$, defined as

$$\mathcal{N}_q = (1 - q)\text{id} + q\mathcal{T}, \quad \rho \mapsto (1 - q)\rho + \frac{q}{d}\mathbb{1} \quad (43)$$

for a noise parameter $q \in [0, 1]$.⁶ Here id denotes the identity channel and \mathcal{T} takes any state to the maximally mixed state $\tau = \mathbb{1}/d$.

A trivial error bound for a circuit as in Fig. 16 can then be found by just calculating the probability of no error occurring at all; disregarding the beneficial effects of a causal lightcone behind the observable O , and denoting with $\mathcal{U} := U_{\text{circ}}^\dagger \cdot U_{\text{circ}}$ the clean circuit, and with \mathcal{U}' the circuit saturated with intermediate errors, we get the expression

$$\epsilon = |\text{Tr}[(\mathcal{U}(\rho) - \mathcal{U}'(\rho))O]| \leq 1 - (1 - q)^V, \quad (44)$$

where V is the circuit's volume (i.e. the number of \mathcal{E} interspersed in \mathcal{U}'). It is clear to see that this error bound asymptotically approaches 1, and does so exponentially quickly. Thus, to stay below a target error rate ϵ_{tar} , a sufficient condition is that

$$1 - (1 - q)^V < \epsilon_{\text{tar}} \iff V < \log \left(\frac{1 - \epsilon_{\text{tar}}}{1 - q} \right), \quad (45)$$

or alternatively

$$\iff q < 1 - \sqrt[V]{1 - \epsilon_{\text{tar}}}. \quad (46)$$

Instead of assuming that each error channel \mathcal{E} in Fig. 16 has the same error probability q , we can analyse the case where q is proportional to the pulse length of the preceding or anteceding gate; corresponding relations as given in Eqs. (45) and (46) can readily be derived numerically.

6.6 Error Mapping under Fermionic Encodings

In [Bau+20b], the authors analyse how noise on the physical qubits translates to errors in the fermionic code space. To first order and in the W3 encoding, all of $\{X, Y, Z\}$ errors on the face, and $\{X, Y\}$ on the vertex qubits can be detected. Z errors on the vertex qubits – as evident from the form of $h_{\text{on-site}}$ from Eq. (39) – result in an undetectable error; as shown in [Bau+20b, Sec. 3.2], this Z error induces fermionic phase noise.

It is therefore a natural extension to the notion of simulation to allow for *some* errors occur – if they correspond to physical noise in the fermionic space. And indeed, as discussed more extensively in [Bau+20b, Sec. 2.4], phase noise is a natural setting for many fermionic condensed matter systems coupled to a phonon bath [Ng15; Kau+20; Zha+17; MF16; OT05; FF04; SD93] and [Rib14, Ch. 6.1&eq. 6.17].

⁶Strictly speaking \mathcal{N}_q defines a completely positive trace preserving map for all $p \leq 1 + 1/(d^2 - 1)$. We emphasize that the error analysis which follows also works for a more general channel than the depolarizing one.

Location	Syndrome	Effect
Vertex	X	detectable
	Y	detectable
	Z	detectable
Face (Ancilla)	X	detectable
	Y	detectable
	Z	phase noise

Table 3: Error mapping from first order physical noise to the encoded fermionic code space, under the W3 encoding, by [Bau+20b]. All but Z errors on the faces are detectable; the latter result in fermionic phase noise.

We further assume that we can measure all stabilizers (including a global parity operator) *once at the end of the entire circuit*. It is evident that measuring the stabilizers can be done by dovetailing an at most depth 4 circuit to the end of our simulation – much like measuring the stabilizers of the Toric code. It is thus a negligible overhead to the cost of simulation $\mathcal{T}_{\text{cost}}$.

This means that while the fermionic encodings do not provide error correction, they do allow error detection to some extent; we summarize all first order error mappings in Table 3. This means we can numerically simulate the occurrence of depolarizing noise throughout the circuit, map the errors to their respective syndromes, and classify the resulting detectable errors, as well as non-detectable phase, and non-phase noise.

This means we can analyse $\mathcal{T}_{\text{cost}}$ with a demonstrably suppressed error, by allowing the non-detectable non-phase noise to saturate a target error bound. The resulting simulation is such that it corresponds to a faithful simulation of the fermionic system, but where we allow fermionic phase error occurs – where we emphasize that since detectable non-phase errors occur roughly with the same probability as non-detectable phase errors we know that, in expectation, only $O(1)$ phase error occurs throughout the simulation; in brief, it is not a very noisy simulation after all.

The resulting required depolarizing noise parameters for various FH setups we summarize in Fig. 4, and the resulting postselection probabilities in Fig. 19.

6.7 Numeric Results

We can tighten the preceding analysis in several ways. First of, instead of crudely upper bounding the cost of individual gates we can sum these pulse times exactly. To this end, we use both the explicitly defined Trotter formulae coefficients h_{ij} , and also the exact formulae for the pulse times derived in Section 3.

Secondly, we can use tighter bounds for Trotter error, which take into account the commutation relations between pairs of interactions across Trotter layers H_i , the coefficients defined in

$\mathcal{T}_{\text{cost}}(\mathcal{P}_p(\delta_0)^{T/\delta_0})$		
Encoding	standard	sub-circuit
LW	65,418	2,960
VC	80,810	12,582

Figure 17: A comparison of the best achievable $\mathcal{T}_{\text{cost}}(\mathcal{P}_p(\delta_0)^{T/\delta_0})$ for $L = 5$, $T = 7$ and $\epsilon_t = 0.1$ with $\Lambda = 5$ and $r = 1$. Obtained by comparing product formulas up to 4th order.

$\mathcal{T}_{\text{cost}}(\mathcal{P}_p(\delta_0)^{T/\delta_0})$		
Encoding	standard	sub-circuit
LW	647,749	6,595
VC	800,160	41,770

Figure 18: Using older Trotter bounds from the literature [Chi+17, Prop. F.4.], the same comparison of the best achievable $\mathcal{T}_{\text{cost}}(\mathcal{P}_p(\delta_0)^{T/\delta_0})$ for $L = 5$, $T = 7$ and $\epsilon_t = 0.1$ with $\Lambda = 5$ and $r = 1$. Obtained by comparing product formulas up to 4th order.

Lemma 10. Additionally, we obtain a bound which rewrites the Trotter error as a Taylor series, and then bound the Taylor remainder using methods which usually bound the total Trotter error; which bound is tighter depends on the order p of the formula, and the target simulation time. As explained in Lemma 22, a tighter Trotter error allows us to choose a larger δ while achieving the same error ϵ_t , reducing the total cost of the simulation.

Finally, as explained in Section 6.5, a certain simulation circuit size will determine the amount of stochastic error present within the circuit. We assume that the depolarizing noise precedes each Trotter layer, and is proportional to the layers' pulse times.

The table Fig. 17 compares these numerics for the case of a lattice with $L = 5$ and for a sufficiently long time in terms of units set by the lattice spacing as we assume $v = 1$. So for any L we choose $T = \lfloor \sqrt{2}L \rfloor$. We choose an analytic error of $\epsilon_t = 0.1$ as there is no point making the analytic error smaller than the experimental error present in NISQ-era gates. As the LW encoding results in the smallest time cost we investigate how $\mathcal{T}_{\text{cost}}$ varies with ϵ_t for $L = 3, 5$ and 10 below. In these numerics we choose the order p which minimise $\mathcal{T}_{\text{cost}}$ at each value of T .

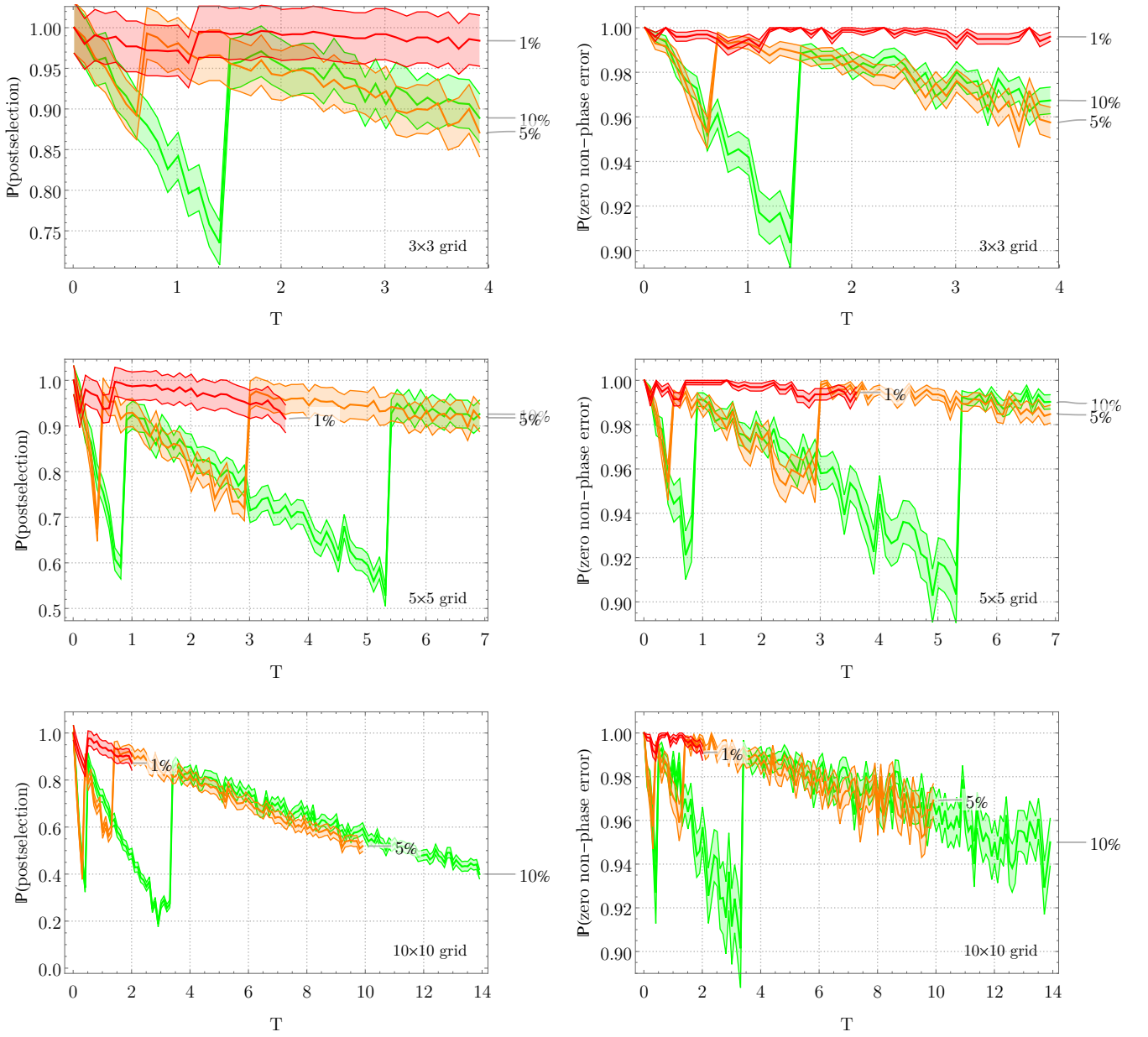


Figure 19: Postselection probabilities (left column) and probability of zero undetectable non-phase error after postselection (right column) for lattice sizes 3×3 , 5×5 , and 10×10 , for the Fermi-Hubbard Hamiltonian H_{FH} from Eq. (2) in the LW encoding, to go alongside Fig. 4. The choice between 1%, 5% and 10% Trotter error is made according to the coloring shown in Fig. 4.

7 Simulating Fermi-Hubbard with Three Trotter Layers

7.1 Further Circuit Decompositions

In this section we show that we can actually simulate a 2D spin Fermi-Hubbard model with $M = 3$ Trotter layers as opposed to the previous $M = 5$. First we need to introduce another circuit decomposition in the spirit as Section 3.

Lemma 25 (Depth 3 Decomposition). *Let $U(t) = e^{it(\cos(\theta)h_1 + \sin(\theta)h_2)}$ be the time-evolution operator for time t under a Hamiltonian $H_\theta = \cos(\theta)h_1 + \sin(\theta)h_2$. If h_1 and h_2 anti-commute and both square to identity, $U(t)$ can be decomposed as*

$$U(t) = e^{it_1 h_1} e^{it_2 h_2} e^{it_1 h_1} \quad (47)$$

where the pulse times t_1, t_2 as a function of the target time t are given by

$$t_1 = \frac{1}{2} \tan^{-1} \left(\pm \frac{\cos(t)}{\sqrt{1 - \sin^2(\theta) \sin^2(t)}}, \pm \frac{\cos(\theta) \sin(t)}{\sqrt{1 - \sin^2(\theta) \sin^2(t)}} \right) + \pi c$$

$$t_2 = \tan^{-1} \left(\pm \sqrt{1 - \sin^2(\theta) \sin^2(t)}, \pm \sin(\theta) \sin(t) \right) + 2\pi c$$

where $c \in \mathbb{Z}$ and signs are taken consistently throughout.

Proof. Since h_1, h_2 square to identity by assumption, we have

$$e^{it_1 h_1} e^{it_2 h_2} e^{it_1 h_1} = \mathbb{1} \cos(2t_1) \cos(t_2) + i h_1 \sin(2t_1) \cos(t_2) + i h_2 \sin(t_2),$$

and

$$e^{it(\cos(\theta)h_1 + \sin(\theta)h_2)} = \mathbb{1} \cos(t) + i \sin(t) (\cos(\theta)h_1 + \sin(\theta)h_2).$$

Equating these and solving for t_1 and t_2 gives the expressions in the Lemma. \square

We then need to establish the overhead associated with implementing this decomposition. We will see that for a target time t , the pulse times in Lemma 25 are as $t_i(t) \propto t$.

Lemma 26. *Let $H = \cos(\theta)h_1 + \sin(\theta)h_2$ be as in Lemma 25. For $0 \leq t \leq \pi/2$ and $0 < \theta < \pi/2$, the pulse times t_1, t_2 in Lemma 25 can be bounded by*

$$|t_1| \leq \frac{t}{2},$$

$$|t_2| \leq t\theta.$$

Proof. Lemma 25 gives two valid sets of solutions for t_1, t_2 . Choose the following solution:

$$t_1 = \frac{1}{2} \tan^{-1} \left(\frac{\cos(t)}{\sqrt{1 - \sin^2(\theta) \sin^2(t)}}, \frac{\cos(\theta) \sin(t)}{\sqrt{1 - \sin^2(\theta) \sin^2(t)}} \right)$$

$$t_2 = \tan^{-1} \left(\sqrt{1 - \sin^2(\theta) \sin^2(t)}, \sin(\theta) \sin(t) \right).$$

Taylor expanding these functions about $t = 0$ and $\theta = 0$, we have

$$t_1 = \frac{t}{2} + R_1(t, \theta),$$

$$t_2 = t\theta + R_2(t, \theta),$$

Basic calculus shows that the Taylor remainders R_1, R_2 are always negative for the stated range of t , giving the stated bounds. \square

7.2 Regrouping Interaction Terms

Now we apply this and the previous decompositions to simulate H_{FH} as encoded using the LW encoding, using only three Trotter layers: $\{H_0, H_1, H_2\}$. The first of these layers consists of all the on-site interactions:

$$H_0 := \frac{u}{4} \sum_{i=1}^N (\mathbb{1} - Z_{i\uparrow}) (\mathbb{1} - Z_{i\downarrow}), \quad (48)$$

and the other two layers are a *mix* of horizontal and vertical hopping terms. Each has the same form, but consists of different sets of interactions as shown in Fig. 20.

$$H_{1/2} := +\frac{v}{2} \sum_{i < j} \sum_{\sigma \in \{\uparrow, \downarrow\}} (X_{i,\sigma} X_{j,\sigma} Y_{f(i,j),\sigma} + Y_{i,\sigma} Y_{j,\sigma} Y_{f(i,j),\sigma}) \quad (49)$$

$$+ \frac{v}{2} \sum_{i < j} \sum_{\sigma \in \{\uparrow, \downarrow\}} g(i, j) (X_{i,\sigma} X_{j,\sigma} X_{f(i,j),\sigma} + Y_{i,\sigma} Y_{j,\sigma} X_{f(i,j),\sigma}). \quad (50)$$

Now we show that $e^{i\delta H_1}$ can be implemented directly; the case of $e^{i\delta H_2}$ follows similarly. As H_1 consists of interactions on disjoint sets of qubits, each forming a square on four qubits in Fig. 20, we only need to show that we can implement evolution under the interactions making up one of the squares. We will denote these by h_i . We will label an example h_1 as shown in Fig. 21 and demonstrate that this can be done. Using this labelling, the square of interactions is given by

$$h_1 = \frac{1}{2} (X_1 X_2 + Y_1 Y_2) Y_a + \frac{1}{2} (X_3 X_4 + Y_3 Y_4) Y_a \quad (51)$$

$$+ \frac{1}{2} (X_1 X_4 + Y_1 Y_4) X_a - \frac{1}{2} (X_2 X_3 + Y_2 Y_3) X_a. \quad (52)$$

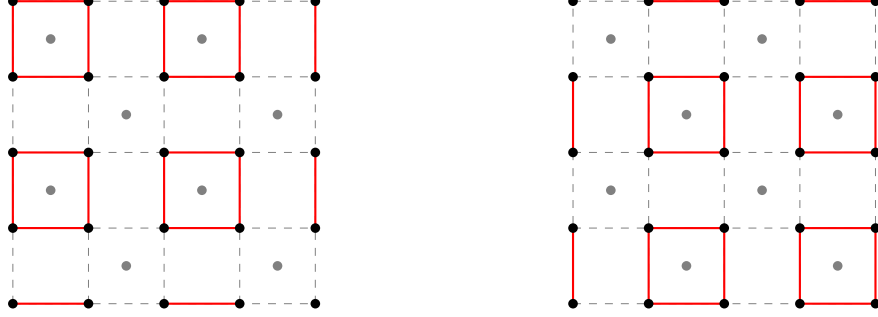


Figure 20: The interactions in H_1 (left) and those in H_2 (right). Gray nodes represent ancillary qubits, all non-gray qubits encode fermionic sites of a particular spin.

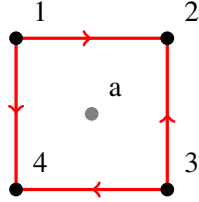


Figure 21: The Hamiltonian h_1 : a *sum* of each Pauli interaction represented by a red line connecting a pair of qubits. Upward pointing arrows indicate $g(i, j) = -1$ and downward, left and right pointing arrows indicate $g(i, j) = 1$ (See [DK20]). H_1 is a sum of disjoint Hamiltonians of this form, shown in Fig. 20

Now we will regroup these interactions in such way that we can use the methods of Section 3 and Lemma 25 to decompose $e^{i\delta h_1}$. To do this we group the terms as $h_1 = a_1 + a_2 + b_1 + b_2$, where

$$a_1 = \frac{1}{\sqrt{2}} \left(\frac{X_1 X_2 Y_a - X_a X_2 X_3}{\sqrt{2}} \right) \quad (53)$$

$$a_2 = \frac{1}{\sqrt{2}} \left(\frac{Y_1 Y_4 X_a + Y_a Y_4 Y_3}{\sqrt{2}} \right) \quad (54)$$

$$b_1 = \frac{1}{\sqrt{2}} \left(\frac{Y_1 Y_2 Y_a - X_a Y_2 Y_3}{\sqrt{2}} \right) \quad (55)$$

$$b_2 = \frac{1}{\sqrt{2}} \left(\frac{X_1 X_4 X_a + Y_a X_4 X_3}{\sqrt{2}} \right). \quad (56)$$

We have reordered terms in order to easily verify the following commutation and anti-commutation relations: (i). Every a_i and b_i squares to something proportional to the identity and consists of two anti-commuting Pauli terms. (ii). The only pairs of a_i and b_i which don't commute, instead anti-commute:

$$\{a_1, b_2\} = 0$$

$$\{a_2, b_1\} = 0.$$

It is easy to verify that all other pairs of a_i and b_i commute. This allows us to implement the target evolution as follows

$$e^{i\delta h_1} = e^{i\delta(a_1+b_2)} e^{i\delta(a_2+b_1)}. \quad (57)$$

Now we only need to show that we can implement $e^{i\delta(a_1+b_2)}$; the implementation of $e^{i\delta(a_2+b_1)}$ follows similarly. Consider the Hamiltonian

$$a_1 + b_2 = \frac{1}{\sqrt{2}} \left(\frac{X_1 X_2 Y_a - X_a X_2 X_3}{\sqrt{2}} \right) + \frac{1}{\sqrt{2}} \left(\frac{X_1 X_4 X_a + Y_a X_4 X_3}{\sqrt{2}} \right). \quad (58)$$

This meets the criteria to decompose $e^{i\delta(a_1+b_2)}$ with two applications of Lemma 25. The first application gives the decomposition

$$e^{i\delta(a_1+b_2)} = e^{it_1 \frac{X_1 X_2 Y_a - X_a X_2 X_3}{\sqrt{2}}} e^{it_2 \frac{X_1 X_4 X_a + Y_a X_4 X_3}{\sqrt{2}}} e^{it_1 \frac{X_1 X_2 Y_a - X_a X_2 X_3}{\sqrt{2}}} \quad (59)$$

where the pulse times are a function of the target time $t_i = t_i(\delta)$ as defined in Lemma 25. Then we apply Lemma 25 again, to each of the individual gates in Eq. (59). The first gate in Eq. (59) decomposes as

$$e^{it_1 \frac{X_1 X_2 Y_a - X_a X_2 X_3}{\sqrt{2}}} = e^{t_1(t_1) X_1 X_2 Y_a} e^{t_2(t_1) X_a X_2 X_3} e^{t_1(t_1) X_1 X_2 Y_a}, \quad (60)$$

and the others decompose similarly. Now we need only apply Lemma 6 to decompose these three qubit unitaries into evolution under two-local Pauli interactions. As Lemma 26 shows that up until now the pulse times have remained $\propto \delta$, it is only this final step which introduces a root overhead. Hence the run-time remains asymptotically as Remark 24.

Acknowledgements

The authors thank Joel Klassen for providing the proof in Section 5, and for many useful discussions.

References

- [Vil+20] Benjamin Villalonga, Dmitry Lyakh, Sergio Boixo, Hartmut Neven, Travis S. Humble, Rupak Biswas, Eleanor Rieffel, Alan Ho, and Salvatore Mandra. “Establishing the quantum supremacy frontier with a 281 Pflop/s simulation”. *Quantum Science and Technology* (Mar. 2020). arXiv: 1905.00444.
- [BJS11] Michael J. Bremner, Richard Jozsa, and Dan J. Shepherd. “Classical simulation of commuting quantum computations implies collapse of the polynomial hierarchy”. *Proceedings of the Royal Society A: Mathematical, Physical and Engineering Sciences* 467.2126 (Feb. 2011), pp. 459–472.
- [AA10] Scott Aaronson and Alex Arkhipov. “The Computational Complexity of Linear Optics”. *Theory of Computing* 9.1 (Nov. 2010), pp. 143–252. arXiv: 1011.3245.
- [BMS17] Michael J. Bremner, Ashley Montanaro, and Dan J. Shepherd. “Achieving quantum supremacy with sparse and noisy commuting quantum computations”. *Quantum* 1 (Apr. 2017), p. 8. arXiv: 1610.01808.
- [HM17] Aram W. Harrow and Ashley Montanaro. “Quantum computational supremacy”. *Nature* 549.7671 (Sept. 2017), pp. 203–209.
- [Goo+19a] Quantum AI Lab Google et al. “Quantum supremacy using a programmable superconducting processor”. *Nature* 574.7779 (Oct. 2019), pp. 505–510.
- [Pre12] John Preskill. “Quantum computing and the entanglement frontier” (Mar. 2012). arXiv: 1203.5813.
- [Pre18] John Preskill. “Quantum Computing in the NISQ era and beyond”. *Quantum* 2 (Aug. 2018), p. 79.
- [HRS16] Thomas Häner, Martin Roetteler, and Krysta M. Svore. “Factoring using $2n+2$ qubits with Toffoli based modular multiplication” (Nov. 2016). arXiv: 1611.07995.
- [Roe+17] Martin Roetteler, Michael Naehrig, Krysta M. Svore, and Kristin Lauter. “Quantum Resource Estimates for Computing Elliptic Curve Discrete Logarithms”. In: 2017, pp. 241–270.
- [Mon15] Ashley Montanaro. “Quantum walk speedup of backtracking algorithms” (2015), pp. 1–23. arXiv: 1509.02374.

- [Fey82] Richard P. Feynman. “Simulating physics with computers”. *International Journal of Theoretical Physics* 21.6-7 (June 1982), pp. 467–488.
- [Llo96] S. Lloyd. “Universal Quantum Simulators”. *Science* 273.5278 (Aug. 1996), pp. 1073–1078.
- [Kiv+19] Ian D Kivlichan, Craig Gidney, Dominic W Berry, Nathan Wiebe, Jarrod McClean, Wei Sun, Zhang Jiang, Nicholas Rubin, Austin Fowler, Alán Aspuru-Guzik, et al. “Improved fault-tolerant quantum simulation of condensed-phase correlated electrons via Trotterization” (2019). arXiv: 1902.10673.
- [Kit97] A Yu Kitaev. “Quantum computations: algorithms and error correction”. *Russian Mathematical Surveys* 52.6 (Dec. 1997), pp. 1191–1249.
- [DN05] Christopher M. Dawson and Michael A. Nielsen. “The Solovay-Kitaev algorithm” (May 2005). arXiv: quant-ph/0505030.
- [NC10] Michael A. Nielsen and Isaac L. Chuang. *Quantum Computation and Quantum Information*. Cambridge: Cambridge University Press, 2010, p. 676.
- [Goo+19b] Frank Google Arute et al. “Quantum supremacy using a programmable superconducting processor Supplementary information Supplementary information for “Quantum supremacy using a programmable superconducting processor”” (2019).
- [LR72] Elliott H. Lieb and Derek W. Robinson. “The finite group velocity of quantum spin systems”. *Communications in Mathematical Physics* 28.3 (Sept. 1972), pp. 251–257.
- [Bau+20a] Bela Bauer, Sergey Bravyi, Mario Motta, and Garnet Kin-Lic Chan. “Quantum algorithms for quantum chemistry and quantum materials science” (Jan. 2020). arXiv: 2001.03685.
- [LeB+15] J. P. F. LeBlanc et al. “Solutions of the Two Dimensional Hubbard Model: Benchmarks and Results from a Wide Range of Numerical Algorithms”. *Physical Review X* 5.4 (May 2015). arXiv: 1505.02290.
- [Chi+17] Andrew Childs, Dmitri Maslov, Yunseong Nam, Neil Ross, Yuan Su, and Yuan Su. “Toward the first quantum simulation with quantum speedup” (2017).
- [VC05] F. Verstraete and J. I. Cirac. “Mapping local Hamiltonians of fermions to local Hamiltonians of spins”. *Journal of Statistical Mechanics: Theory and Experiment* (Aug. 2005).
- [DK20] Charles Derby and Joel Klassen. “Low Weight Fermionic Encodings for Lattice Models”. 2020.
- [Bau+20b] Johannes Bausch, Toby S. Cubitt, Charles Derby, and Joel Klassen. “Mitigating Errors in Local Fermionic Encodings”. 2020.

- [JW28] P. Jordan and E. Wigner. “Über das Paulische Äquivalenzverbot”. *Zeitschrift für Physik* 47.9-10 (Sept. 1928), pp. 631–651.
- [BK02] Sergey B. Bravyi and Alexei Yu Kitaev. “Fermionic quantum computation”. *Annals of Physics* 298.1 (May 2002), pp. 210–226. arXiv: 0003137 [quant-ph].
- [Ber+15] Dominic W. Berry, Andrew M. Childs, Robin Kothari, and Robin Kothari. “Hamiltonian Simulation with Nearly Optimal Dependence on all Parameters”. In: *2015 IEEE 56th Annual Symposium on Foundations of Computer Science*. IEEE, Oct. 2015, pp. 792–809.
- [LC16] Guang Hao Low and Isaac L. Chuang. “Hamiltonian Simulation by Qubitization” (Oct. 2016). arXiv: 1610.06546.
- [Ber+14] Dominic W. Berry, Andrew M. Childs, Richard Cleve, Robin Kothari, and Rolando D. Somma. “Simulating Hamiltonian dynamics with a truncated Taylor series” (Dec. 2014). arXiv: 1412.4687.
- [CS19] Andrew M Childs and Yuan Su. *Nearly optimal lattice simulation by product formulas*. Tech. rep. 2019. arXiv: 1901.00564v1.
- [Suz92] Masuo Suzuki. “General theory of higher-order decomposition of exponential operators and symplectic integrators”. *Physics Letters A* (1992).
- [Suz91] Masuo Suzuki. “General theory of fractal path integrals with applications to many-body theories and statistical physics”. *Journal of Mathematical Physics* 32.2 (Feb. 1991), pp. 400–407.
- [Kna05] A. W. Knap. *Basic Real Analysis*. Birkhäuser, 2005.
- [PVH13] Tien Trung Pham, Rodney Van Meter, and Clare Horsman. “Optimization of the Solovay-Kitaev algorithm”. *Physical Review A* 87.5 (May 2013), p. 052332.
- [Mar+16] Esteban A Martinez, Thomas Monz, Daniel Nigg, Philipp Schindler, and Rainer Blatt. “Compiling quantum algorithms for architectures with multi-qubit gates”. *New Journal of Physics* 18.6 (June 2016), p. 063029.
- [MN17] Dmitri Maslov and Yunseong Nam. “Basic circuit compilation techniques for an ion-trap quantum machine Related content Use of global interactions in efficient quantum circuit constructions Basic circuit compilation techniques for an ion-trap quantum machine”. *New J. Phys* 19 (2017), p. 23035.
- [Bau+20c] Johannes Bausch, Toby Cubitt, Charles Derby, and Joel Klassen. (to appear). 2020.
- [Ng15] H. T. Ng. “Decoherence of interacting Majorana modes”. *Scientific Reports* 5.1 (July 2015), pp. 1–14. arXiv: 1409.6102.

- [Kau+20] A. Kauch, P. Puddleiner, K. Astleithner, P. Thunström, T. Ribic, and K. Held. “Generic Optical Excitations of Correlated Systems: π -tons”. *Physical review letters* 124.4 (Jan. 2020), p. 047401. arXiv: 1902.09342.
- [Zha+17] Xinyu Zhao, Wufu Shi, J. Q. You, and Ting Yu. “Non-Markovian dynamics of quantum open systems embedded in a hybrid environment”. *Annals of Physics* 381 (June 2017), pp. 121–136. arXiv: 1704.00091.
- [MF16] Alexey A. Melnikov and Leonid E. Fedichkin. “Quantum walks of interacting fermions on a cycle graph”. *Scientific Reports* 6.1 (Sept. 2016), pp. 1–13.
- [OT05] L. A. Openov and A. V. Tsukanov. “Selective electron transfer between quantum dots induced by a resonance pulse”. *Semiconductors* 39.2 (2005), pp. 235–242.
- [FF04] L. Fedichkin and A. Fedorov. *Error rate of a charge qubit coupled to an acoustic phonon reservoir*. Mar. 2004.
- [SD93] Marlan O. Scully and Jonathan P. Dowling. “Quantum-noise limits to matter-wave interferometry”. *Physical Review A* 48.4 (Oct. 1993), pp. 3186–3190.
- [Rib14] Wellington Luiz Ribeiro. “Evolution of a 1D Bipartite Fermionic Chain Under Influence of a Phenomenological Dephasing”. PhD thesis. Universidade Federal do ABC (UFABC), 2014.
- [Chi+19] Andrew M. Childs, Yuan Su, Minh C. Tran, Nathan Wiebe, and Shuchen Zhu. “A Theory of Trotter Error” (Dec. 2019). arXiv: 1912.08854.
- [Kja+19] Morten Kjaergaard, Mollie E. Schwartz, Jochen Braumüller, Philip Krantz, Joel I-Jan Wang, Simon Gustavsson, and William D. Oliver. *Superconducting Qubits: Current State of Play*. 2019. arXiv: 1905.13641 [quant-ph].
- [Pou+11] David Poulin, Angie Qarry, R. D. Somma, and Frank Verstraete. “Quantum simulation of time-dependent Hamiltonians and the convenient illusion of Hilbert space” (Feb. 2011). arXiv: 1102.1360.
- [DBB07] Wolfgang Dür, Michael J Bremner, and Hans J Briegel. *Quantum simulation of interacting high-dimensional systems: the influence of noise*. Tech. rep. 2007. arXiv: 0706.0154v1.
- [Yun+14] Man-Hong Yung, James D. Whitfield, Sergio Boixo, David G. Tempel, and Alán Aspuru-Guzik. “Introduction to Quantum Algorithms for Physics and Chemistry”. In: Mar. 2014, pp. 67–106. arXiv: 1203.1331.
- [Bau12] Johannes Bausch. “On the Efficient Calculation of a Linear Combination of Chi-Square Random Variables with an Application in Counting String Vacua”. *Journal of Physics A: Mathematical and Theoretical* 46.50 (Aug. 2012), p. 505202. arXiv: 1208.2691.

- [KMS01] M. Keller, W. Metzner, and U. Schollwöck. “Dynamical mean-field theory for pairing and spin gap in the attractive Hubbard model”. *Physical Review Letters* 86.20 (May 2001), pp. 4612–4615.
- [KO14] Tatsuya Kaneko and Yukinori Ohta. “BCS-BEC crossover in the two-dimensional attractive hubbard model: Variational cluster approach”. *Journal of the Physical Society of Japan* 83.2 (Feb. 2014). arXiv: 1308.0664.